Constraints on the crustal structure of the internal Variscan Belt in SW Europe: A magnetotelluric transect along the eastern part of Central Iberian Zone, Iberian Massif

Jaume Pous, David Martinez Poyatos, Wiebke Heise, Fernando Monteiro Santos, Jesus Galindo-Zaldivar, Pedro Ibarra, Antonio Pedrera, Ana Ruiz-Constan, Farida Anahnah, Rui Goncalves, et al.

Constraints on the crustal structure of the internal Variscan Belt in SW Europe: A magnetotelluric transect along the eastern part of Central Iberian Zone, Iberian Massif

Jaume Pous,[1] David Martínez Poyatos,[2] Wiebke Heise,[3] Fernando Monteiro Santos,[3] Jesús Galindo-Zaldívar,[2,4] Pedro Ibarra,[5] Antonio Pedrera,[2] Ana Ruiz-Constán,[2] Farida Anahnah,[2] Rui Gonçalves,[6] and Antonio Mateus[7]

Received 11 March 2010; revised 31 October 2010; accepted 24 November 2010; published 15 February 2011.

[1] The Iberian Massif is the best exposed segment of the European Variscan Belt. It includes relatively well preserved terranes that were accreted by transpression along time and resulted in a number of geotectonic units that formed part of the Late Paleozoic assembly of the Pangaea Supercontinent. In SW Iberia, these units are the Central Iberian Zone (CIZ), Ossa Morena Zone (OMZ), and the South Portuguese Zone (SPZ). A 210 km long NE-SW magnetotelluric profile was carried out through the CIZ, from the OMZ-CIZ boundary toward the north, reaching the Tagus (Cenozoic) basin. Data dimensionality analysis resulted in a suitable 2-D electrical resistivity structure, allowing a 2-D inversion of the data set. Complementary available geophysical data (deep seismic, gravity and aeromagnetic) and a comparison with a detailed geological cross section led us to constrain the interpretation of the 2-D electrical resistivity structure of the CIZ crust. The results show, for the upper crust, the existence of diverse conductive/resistive bodies that correlate well with known geological features (sedimentary basins, faults, granitic plutons, mineralized systems). A mild but steady conductive band is located along the middle and lower crust that is interpreted as a mafic granulite basement. The upper section of this band connects with several elongated shallow conductors, providing further evidence for the existence, in the Central Iberian Zone, of a complex décollement system where the major faults are rooted. Such a crustal architecture is viewed as the northward continuation of the Variscan large-scale structures previously recognized in the southern sectors (OMZ and SPZ).

Citation: Pous, J., et al. (2011), Constraints on the crustal structure of the internal Variscan Belt in SW Europe: A magnetotelluric transect along the eastern part of Central Iberian Zone, Iberian Massif, *J. Geophys. Res.*, *116*, B02103, doi:10.1029/2010JB007538.

1. Introduction

[2] The Iberian Massif corresponds to the largest continuous outcrop of the Late Paleozoic Alleghanian/Variscan Orogen in western Europe. Its southern branch comprises three geotectonic units (Figure 1) that, from north to south, are known as the Central Iberian Zone (CIZ), the Ossa Morena Zone (OMZ), and the South Portuguese Zone (SPZ). The two first units represent internal zones of the orogen and were sutured in eo-Variscan times [e.g., *Azor et al.*, 1994; *Matte*, 2001], though a Cadomian (Neoproterozoic) tectonometamorphic record has also been proposed [e.g., *Quesada and Dallmeyer*, 1994; *Ribeiro et al.*, 2007]. The SPZ is a distinct terrane that forms the southern external zone of the Iberian Variscides amalgamated to the OMZ in the course of the Variscan oblique continental collision [e.g., *Figueiras et al.*, 2002; *Ribeiro et al.*, 2007].

[3] The internal architecture of the lithosphere across the southern Iberian Variscides has been the subject of a significant number of geophysical studies since the early work of *Prodehl et al.* [1975] in the SPZ. Seismic refraction and wide-angle reflection data found a flat Moho at ~31 km depth for the southern Iberian Massif [*Banda et al.*, 1981; *Palomeras et al.*, 2009]. A deep seismic reflection profile (IBERSEIS [*Simancas et al.*, 2003; *Carbonell et al.*, 2004])

[1]Departament de Geodinàmica i Geofísica, Universitat de Barcelona, Barcelona, Spain.
[2]Departamento de Geodinámica, Universidad de Granada, Granada, Spain.
[3]Facultade de Ciencias da Universidade de Lisboa, CGUL-IGL, Lisbon, Portugal.
[4]Instituto Andaluz de Ciencias de la Tierra-CSIC, Universidad de Granada, Granada, Spain.
[5]Instituto Geológico y Minero de España, Madrid, Spain.
[6]Instituto Politécnico de Tomar, Tomar, Portugal.
[7]Departamento de Geologia and CeGUL, Faculdade Ciências, Universidade de Lisboa, Lisbon, Portugal.

0148-0227/11/2010JB007538

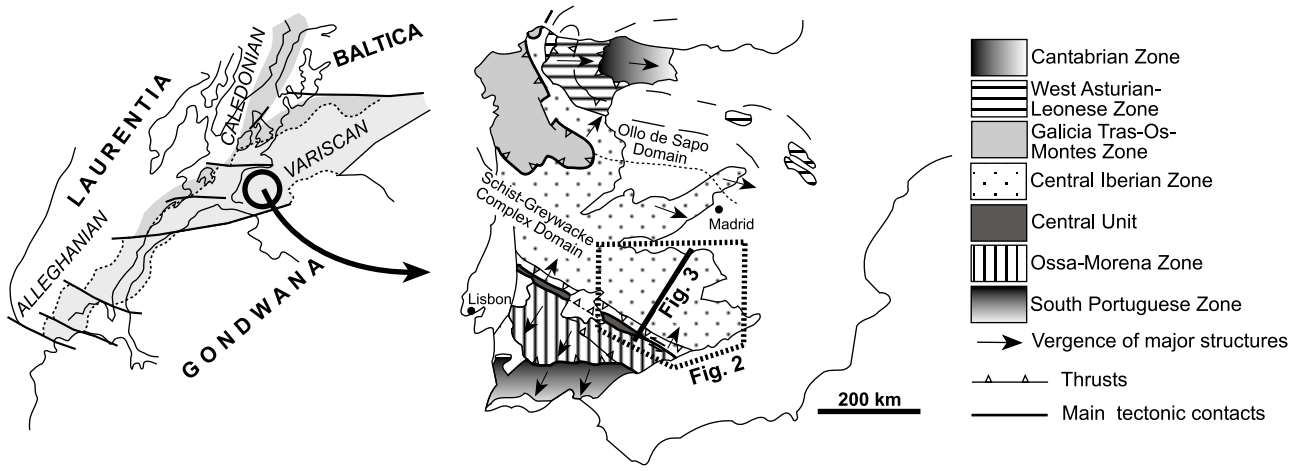

Figure 1. Geotectonic map of the Iberian Massif in the context of the Alleghanian-Variscan Orogeny.

showed a lower crust detached from an imbricate faulted and folded upper crust in the SPZ, OMZ and southernmost CIZ.

[4] The magnetotelluric (MT) method is increasingly being applied to gain fresh insights into the nature, behavior (thermal state, presence of fluids) and structure of a varied range of continental areas. These areas include old cratons (e.g., Slave craton [*Jones et al.*, 2001], Fennoscandia Shield [*Lahti et al.*, 2005], and Dharwar Craton [*Harinarayana et al.*, 2006]), Paleozoic orogens (e.g., Appalachian [*Ogawa et al.*, 1996]) and active subduction (e.g., Andean [*Brasse and Eydam*, 2008]) or collision zones (e.g., India-Asia [*Wei et al.*, 2001; *Unsworth et al.*, 2005]).

[5] Magnetotellurics has also proved to be an efficient technique for imaging old structures affecting rocks that bear (interconnected) conductive mineral phases (e.g., graphite, sulphides, iron oxides). In SW Iberia, five magnetotelluric (MT) profiles provided evidence of the orogenic sutures at depth, which are characterized by high conductivities [*Monteiro Santos et al.*, 1999, 2002; *Almeida et al.*, 2001, 2005; *Pous et al.*, 2004; *Muñoz et al.*, 2005; *Vieira da Silva et al.*, 2007]. A midcrustal conductive layer along the whole OMZ was revealed, suggesting a major middle crust décollement between a granulitic basement and the overlying sequence, mostly composed of metasedimentary and metavolcanic rocks [*Muñoz et al.*, 2008]. These MT profiles, only coming into contact the CIZ, seemed to indicate the presence of this conductive layer also in this geotectonic unit.

[6] In order to investigate the aforementioned issues in the CIZ and obtain additional information about the OMZ-CIZ boundary at depth, a new MT profile was performed. This 210 km long (NE-SW) MT profile across the eastern CIZ (Figure 2) intersects the OMZ-CIZ boundary and extends northward through the Alcudia and the Toledo Mountains, as far as the Tagus basin. The MT measurements were taken together with transient electromagnetic (TEM) soundings in order to control the galvanic distortion and static shift displacement of the apparent resistivities. Since the electrical conductivity of geological units is affected by many factors (such as interstitial aqueous fluids, silicate melts, graphite or other interconnected conductive mineral phases), data interpretation must consider the geodynamic interplay responsible for the present-day arrangement of these units, as well as the critical features displayed by the rocks involved. In this regard, the existence of magnetic, gravity and deep seismic data in the surveyed and nearby areas helped us to interpret the electrical resistivity image obtained from MT data. Additionally, for the shallow crust, a detailed comparison with an accurate geological cross section along the MT profile enabled the recognition of several structural/lithological finger prints. As a result, there is an improvement in the interpretation and moreover the usefulness of the MT method in resolving such complex geological frameworks is shown.

2. Geodynamic Setting

[7] The studied section crosses an important segment of the Iberian Massif (Figure 1), which is part of the Alleghanian/Variscan fold-thrust orogenic belt generated through oblique continental collision after subduction and closure of the Rheic Ocean (Lower/Middle Devonian) that separated Laurentia/Baltica and Gondwana continents since the Ordovician [e.g., *von Raumer et al.*, 2002; *Nance et al.*, 2010]. In short, that collision (Upper Devonian – Pennsylvanian) amalgamated those continents along with minor oceanic-like and ribbon-continental domains, developing an intricate architecture whose main components are separated by first-order lithospheric structures [e.g., *Franke*, 2000]. Later on, the opening of the Atlantic Ocean and the Alpine orogeny reworked and dispersed the Paleozoic orogen into several portions that now crop out in western Europe, northwest Africa and northeast America.

[8] The Iberian Massif (Figure 1) exposes a complete section across the Variscan Belt, from the SPZ in the south, through the internal zones (OMZ, CIZ, Galicia-Trás-os-Montes and West Asturian Leonese zones) to the external Cantabrian Zone in the north [e.g., *Julivert et al.*, 1972]. The CIZ, West Asturian Leonese and Cantabrian zones are continental domains that once formed part of a wide passive margin in northern Gondwana during the Early Paleozoic (prior to the Variscan orogeny). The OMZ is commonly interpreted as a ribbon continental domain rifted from Gondwana (i.e., the CIZ) in the Early Paleozoic [*Matte*, 2001]. Subsequent oblique collision between the OMZ and

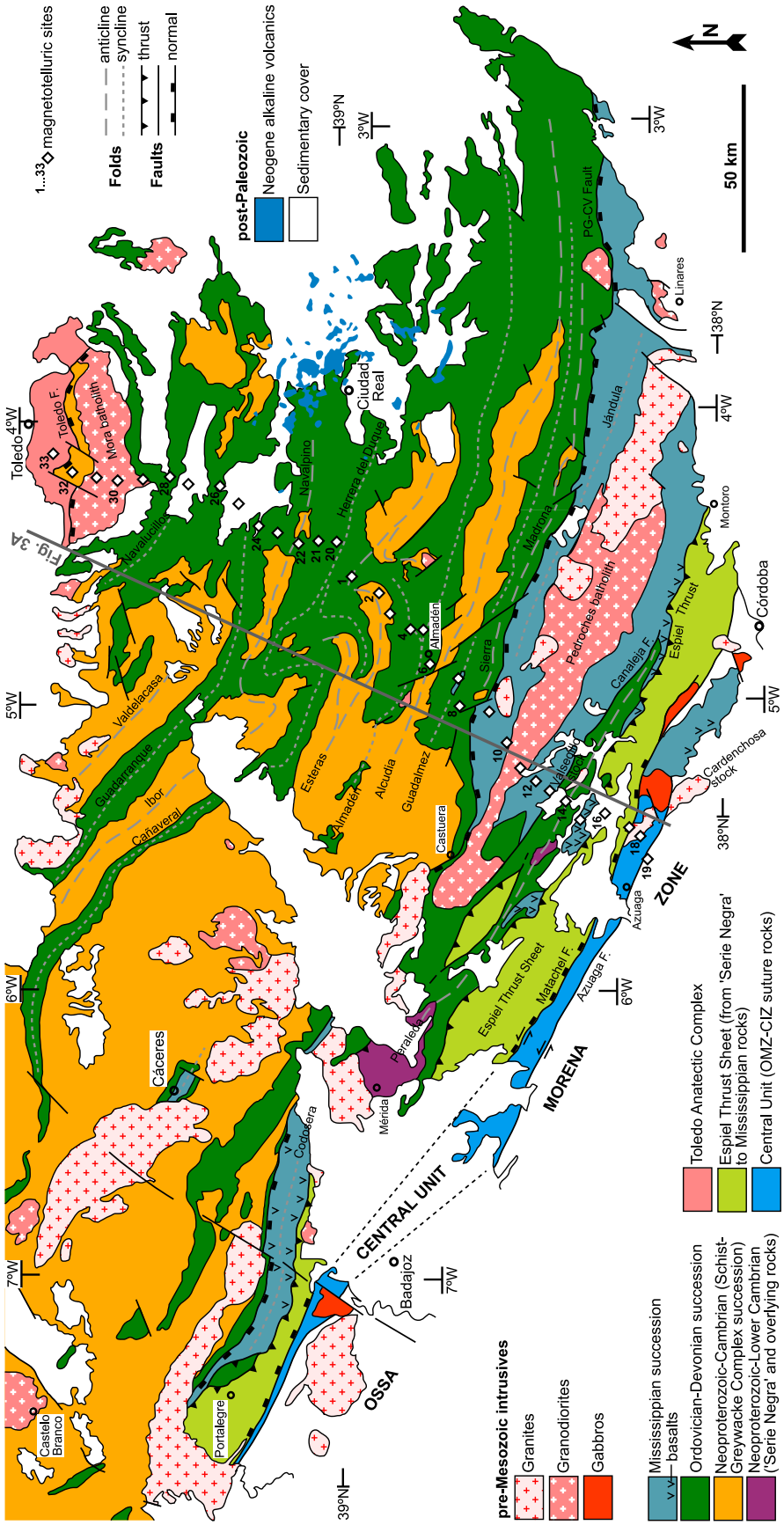

Figure 2. Geological map of the studied area. The geological cross section and the magnetotelluric profile (numbered sites) of Figure 3 are located. Abbreviations are as in Figure 3c.

the CIZ in the Late Paleozoic resulted in the suture known as the Portalegre-Badajoz-Córdoba Shear Zone [*Burg et al.*, 1981] or Central Unit [*Azor et al.*, 1994]. Following oceanic consumption, the SPZ collided with the OMZ in the Late Paleozoic, although it is unclear whether the former really represents part of the Avalonia (Laurentia) continent [*Tait et al.*, 2000].

[9] The CIZ is subdivided into two tectonic domains with contrasting structural styles and lithostratigraphic features [*Martínez Catalán et al.*, 2004] (Figure 1): a northern one (Ollo de Sapo Domain, characterized by Ordovician glandular gneisses and Variscan recumbent folds) and a southern one (Schist-Graywacke Complex Domain). The southern domain is characterized by a thick Neoproterozoic–Lower Cambrian flysch sedimentary succession (Schist-Graywacke Complex) and Variscan upright folds. The new MT profile crisscrosses a representative section of the Schist-Graywacke Complex Domain (Figure 2), which to the north is covered by the Madrid-Toledo Cenozoic Basin (also known as the Tagus basin); the southern end of this profile is located in the Central Unit, thus reaching the OMZ.

3. The Geological Cross Section Along the MT Profile

3.1. The OMZ-CIZ Suture

[10] The Central Unit (Figure 3a), separating the OMZ from the CIZ, is a ≥5 km thick tectonic sheet that dips toward the northeast and comprises highly sheared migmatitic orthogneisses and paragneisses, schists as well as amphibolites and partially retrograded eclogite lenses [*Azor et al.*, 1994]. Some of the amphibolites are Lower Paleozoic in age and show an oceanic crust-like geochemical signature [*Gómez-Pugnaire et al.*, 2003].

[11] The Central Unit was imaged by the IBERSEIS seismic reflection profile (located 100 km to the west of our study area [*Simancas et al.*, 2003]) as a northeast dipping reflective wedge in the upper crust. This downdip wedge continues to a midcrustal detachment, and its top is truncated by the late developed Matachel Fault. To the south, the Central Unit is separated from the OMZ by the Late Variscan Azuaga Fault, which at surface appears as a subvertical discontinuity (Figure 3a).

3.2. Stratigraphy

[12] The main geological features of the Schist-Graywacke Complex Domain include (1) a thick Neoproterozoic–Lower Cambrian synorogenic sedimentary succession ("Alcudian") related to the denudation of a Cadomian orogenic belt, (2) an Ordovician to Devonian shallow marine siliciclastic succession developed in a passive margin continental platform of Gondwana, (3) a thick Mississippian synorogenic sedimentary succession (a "Culm" facies basin located in the southern part of the domain) related to extensional tectonics during the Variscan orogeny, (4) upright folding at very low grade metamorphic conditions, (5) widespread granitic plutonism, peaking at circa 320–300 Ma, and (6) late Variscan faulting.

[13] The oldest outcropping rocks in the OMZ and southernmost CIZ are known as the Serie Negra Group, late Neoproterozoic in age. This group consists of a thick (>3000 m) sequence comprising graphite-rich schists, slates and metagraywackes with black quartzites, amphibolites and minor marble intercalations. By sectors, the Serie Negra is overlain by the Vendian–Lower Cambrian Malcocinado Formation, a calc-alkaline metavolcaniclastic succession (rhyolitic to andesitic in composition) that also includes minor metabasalts and some granitoid bodies (e.g., the small Valsequillo stock located in the core of the Peraleda anticline; Figure 2). The Serie Negra Group and the Malcocinado Formation are covered by Cambrian metasandstones, metalimestones, and slates. The core of the Peraleda anticline (Figures 2 and 3) is the northeastern outcrop of these OMZ-type Neoproterozoic rocks.

[14] To the north of the Pedroches area, the oldest outcropping rocks are those belonging to the Schist-Graywacke Complex (or "Alcudian" succession), Vendian to Lower Cambrian in age. This complex is commonly subdivided into Lower Alcudian, Upper Alcudian and Pusian Groups, separated by unconformities; total thickness can exceed 15,000 m although the reported values vary by sectors according to different authors. The Lower Alcudian succession is a monotonous flyschoid alternation of slates and metagraywackes with some metaconglomerates and minor metavolcanic rocks. The overlying sequence is mainly composed of slates occasionally interbedded with black shales, metaconglomerates, metasandstones, metalimestones, phosphate-rich levels and metavolcanic rocks; this Group is covered by Cambrian metasandstones and metalimestones.

[15] The stratigraphic relationship between the Serie Negra Group and the Alcudian succession remains unsolved. It has been argued that the former could extend northward of the Pedroches area, underlying the latter [*Martínez Poyatos et al.*, 2001a], but a lateral facies change was also proposed [*Vidal et al.*, 1994].

[16] The Ordovician to Devonian siliciclastic succession overlies unconformable the previous lithostratigraphic column. It corresponds to a 3000 m thick sequence of alternating quartzite and slaty formations deposited in a shallow marine platform, where the Armorican Quartzite Formation (Lower Ordovician) stands up as a 500 m thick reference. The Lower Silurian (graphite-rich) black shales, forming a 100 m thick series, are also noteworthy. In the Almadén area, local alkaline basaltic magmatism produced diatreme (pyroclastic)-like bodies, sills and lavas, with ultramafic xenoliths, in the Silurian-Devonian succession; their alteration produced Ca-Mg-Fe carbonates, pyrite and cinnabar

Figure 3. (a) Geological cross section of the eastern Schist-Graywacke Complex Domain (modified from *Martínez Poyatos et al.* [2004]) with the approximate projected location (according to direction of structures) of the MT sites. (b) Bouguer and magnetic anomalies (extracted from *IGN* [1976] and *Ardizone et al.* [1989]) along the MT profile.(c) Two-dimensional electrical resistivity model along the MT profile with indication of the main high-resistive and high-conductive zones and geological structures discussed in the text. R, resistive zones; C, conductive zones; SN, conductive Serie Negra Group.

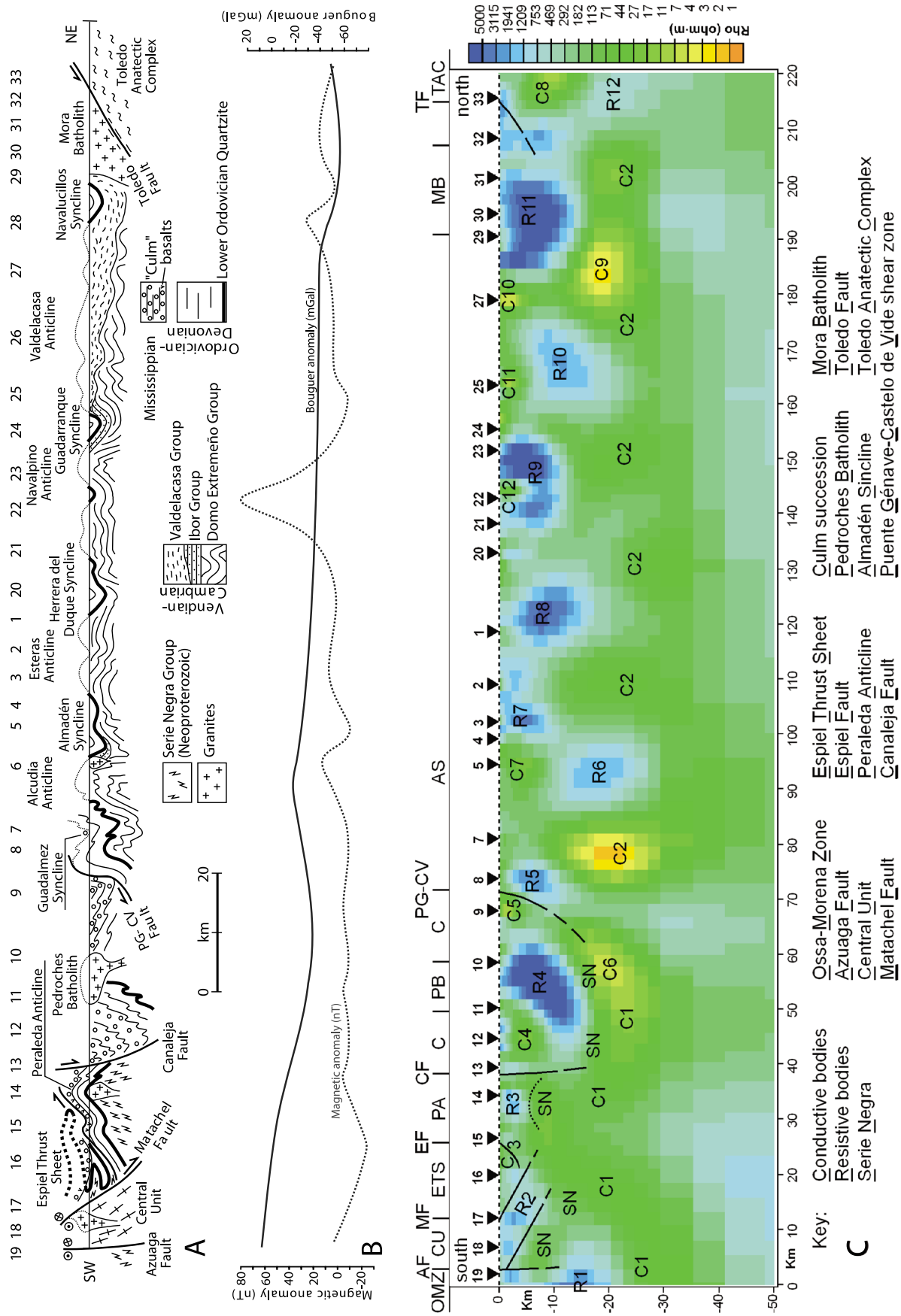
A
B
C
SW
NE
Espiel Thrust Sheet
Peraleda Anticline
Pedroches Batholith
Guadalmez Syncline
Alcudia Anticline
Almadén Syncline
Esteras Anticline
Herrera del Duque Syncline
Navalpino Anticline
Guadarranque Syncline
Valdelacasa Anticline
Navalucillos Syncline
Mora Batholith
Toledo Fault
Toledo Anatectic Complex
Azuaga Fault
Central Unit
Matachel Fault
Canaleja Fault
PG-CV Fault
Serie Negra Group (Neoproterozoic)
Granites
Vendian-Cambrian
Valdelacasa Group
Ibor Group
Domo Extremeño Group
Mississippian
"Culm" basalts
Ordovician-Devonian
Lower Ordovician Quartzite
Magnetic anomaly (nT)
Bouguer anomaly (mGal)
Rho (ohm·m)
south
north
AF
OMZ
CU
MF
ETS
EF
PA
CF
C
PB
PG-CV
AS
MB
TF
TAC
Key:
Conductive bodies
Resistive bodies
Serie Negra
Ossa-Morena Zone
Azuaga Fault
Central Unit
Matachel Fault
Espiel Thrust Sheet
Espiel Fault
Peraleda Anticline
Canaleja Fault
Culm succession
Pedroches Batholith
Almadén Sincline
Puente Génave-Castelo de Vide shear zone
Mora Batholith
Toledo Fault
Toledo Anatectic Complex

Figure 3

mineralizations that host a mercury world class ore system [*Higueras et al.*, 2000].

[17] In the southern CIZ, remarkable Mississippian synorogenic sedimentation ("Culm" facies) is recorded in the Guadiato-Pedroches Basin, best exposed in the Pedroches area where it is known as the "Culm of Pedroches." It is made up of monotonous alternations of dark slates and metagraywackes that, toward the base, also include horizons of metaconglomerates, metavolcanic rocks, and minor metalimestones. Total thickness of this sequence has been estimated to be a minimum of 6000 m, providing evidence for a significant subsidence that can be explained by extension coeval to the exhumation of the previously deep-seated rocks of the Central Unit [*Martínez Poyatos*, 2002]. Contemporary igneous activity took place in the southern part of the Guadiato-Pedroches Basin (as well as in the OMZ and SPZ), where two major outcrops of mafic rocks occur: (1) up to 2000 m of basaltic lavas in the southern limb of the Peraleda Anticline and (2) a gabbroic body that conceals, along with the Mississippian metasediments and granites, the Central Unit toward the east (Figure 2).

3.3. Structure

[18] As regards the structural features, eo-Variscan deformation was restricted to the Espiel Thrust Sheet, located immediately to the north of the Central Unit. The Espiel Thrust Sheet records Devonian NE vergent recumbent folds and associated ductile shearing. Following unconformable Mississippian sedimentation, it thrusts to the NE (the Espiel Thrust) onto their relative CIZ para-authochthon [*Martínez Poyatos et al.*, 1998]. In the Schist-Graywacke Complex Domain, the most outstanding Variscan structures at regional scale are upright to slightly south verging folds (Figure 3a). They formed with associated slaty cleavage under very low grade metamorphic conditions during the Pennsylvanian. These folds usually strike NW-SE, but in a sector NE of Almadén they rotate to a N-S direction as a result of a swivel imposed by a N130°E subvertical left-lateral shear zone [*Ortega*, 1986]. From south to north, the first-order folds are the Peraleda, Pedroches, Alcudia, Esteras, Navalpino and Valdelacasa anticlines, and the intervening Guadalmez, Almadén, Herrera del Duque, Guadarranque and Navalucillos synclines (Figures 2 and 3a).

[19] Late granite genesis/emplacement and faulting (usually of strike-slip type but also with normal kinematics) are the main records of the late Variscan orogenic evolution during the Pennsylvanian-Permian period. Synorogenic to postorogenic granites are very abundant in the CIZ, mainly in its northwestern sector; in the southeast, relevant batholiths are those of Pedroches and Mora (Figure 2), the former comprising a granodioritic pluton intruded by granitic bodies.

[20] Late Variscan left-lateral and normal faults characterize the southern Iberian Massif. From south to north, we are concerned with those of Azuaga, Matachel, La Canaleja, Puente Génave–Castelo de Vide (PG-CV), and Toledo faults (Figure 3a). The Azuaga Fault is a brittle, left-lateral strike-slip fault that bounds the Central Unit to the south, and conceals the original thrust that juxtaposed the Central Unit onto the underlying OMZ. The Matachel Fault is a brittle, north dipping low-angle normal fault that bounds the Central Unit to the north, contributing to its exhumation [*Azor et al.*, 1994]. The Canaleja Fault is a brittle subvertical fault that down threw the northern block [*Martínez Poyatos et al.*, 2001a]. The PG-CV Fault is a ductile to brittle, south dipping shear zone, which has been proposed as the limit that separates a southern crustal domain (with some distinctive geological features) from the remaining Schist-Graywacke Complex Domain [*Martín Parra et al.*, 2006]. The Toledo Fault [*Hernández Enrile*, 1991] has a low dip to the south and exhumed the Toledo Anatectic Complex, a migmatitic dome composed of granulite-grade (800°C, 5 kbar) pelitic migmatites and related granitoids with minor gabbros [*Barbero*, 1995].

4. Previous Geophysical Data

[21] General gravimetric and magnetic surveys are available in the study area: the 1:1,000,000 Bouguer anomaly map [*Instituto Geográfico Nacional* (*IGN*), 1976] and the 1:1,000,000 aeromagnetic anomaly map (at 3 km altitude) of the Spanish National Institute of Geography [*Ardizone et al.*, 1989]. The 1:1,000,000 Bouguer anomaly map reveals wide negative anomalies related to the outcropping igneous bodies (Pedroches and Mora batholiths; Figure 3b) and to the sedimentary basins crossed by the MT profile or located in nearby areas. However, the map is not accurate enough to determine in detail the structure of those batholiths and basins; only the geometry of the small-sized Cardenchosa granite (located near the southernmost end of the profile), extending ~2 km deep and displaying a subhorizontal bottom, is well constrained by a detailed gravity survey [*Simancas et al.*, 2000]. The 1:1,000,000 aeromagnetic map shows numerous WNW-ESE elongated anomalies, parallel to the main Variscan structural trend, which could reflect the presence of hidden mafic/intermediate igneous bodies and/or local enrichments in (ferro-) magnetic ores (Figure 3b). In addition, a detailed anisotropy of magnetic susceptibility research was developed in the Pedroches batholith, providing evidence of subhorizontal magnetic foliations and a thin (<5 km) sheeted laccolith morphology with prevailing horizontal extensions [*Aranguren et al.*, 1997].

[22] In the surveyed area, the main crustal features were established from deep seismic refraction profiles, indicating a flat Moho located at ~31 km depth and an internal structure formed by several flat layers, some of them including velocity inversion [*Banda et al.*, 1981]. More recent deep seismic profiles have significantly improved the crustal image of the SW Iberian Variscides. The IBERSEIS reflection profile [*Simancas et al.*, 2003; *Carbonell et al.*, 2004], located 100 km to the west and south of the new MT survey, imaged a reflective SPZ, OMZ and southernmost CIZ lower crust, detached from the upper crustal levels. Additionally, in the middle crust of the OMZ (and to a lesser extent of the southernmost CIZ), a roughly flat and 2 s thick highly reflective band (known as the Iberian Reflective Body) was observed and interpreted as a Mississippian (intra-Variscan extensional stage) complex sill-like mafic intrusion superposed to the midcrustal detachment. More recently, a wide-angle seismic experiment, partially coincident with the IBERSEIS profile, showed high wave velocities (including velocity inversions) from 15 km to Moho depth in the SPZ, OMZ and southern CIZ, that have

been interpreted as corresponding to a lower crustal mafic granulite basement with mafic intrusions, detached from a metasedimentary upper crust with granitic intrusions [*Palomeras et al.*, 2009]. The very recent ALCUDIA reflection profile, which coincides with the new MT survey, is still being processed. However, a preliminary (stacked) image obtained reveals a highly reflective lower crust beneath a rather transparent upper crust, the midcrustal reflective band not being observed [*Tejero et al.*, 2008].

[23] Five previous parallel NE-SW MT profiles were acquired during the last decade in SW Iberia spanning the SPZ and OMZ, and reaching the CIZ to the north, [*Monteiro Santos et al.*, 1999; *Almeida et al.*, 2001, 2005; *Pous et al.*, 2004; *Vieira da Silva et al.*, 2007; *Muñoz et al.*, 2005, 2008]. These surveys provided evidence of the sutures at depth characterized by high-conductivity anomalies. In particular, the OMZ-CIZ boundary was correlated with a NW-SE conductor extending for more than 220 km. A midcrustal conductive layer along the whole OMZ was detected and interpreted as a major décollement between the granulitic basement and the overlying metasedimentary pile [*Muñoz et al.*, 2008]; this conductive layer shows a spatial correspondence with the Iberian Reflective Body. Furthermore, based on the available data, a similar conductive layer in the CIZ was inferred [*Muñoz et al.*, 2008], prompting us to carry out the new profile within this geotectonic unit.

5. New Magnetotelluric Data

[24] The new MT profile consists of thirty three magnetotelluric sites spaced 5–7 km along a NE-SW direction for ~210 km (Figure 2). Instrumentation at sites 6, 26 and 28 did not work properly and their data have been discarded. The data were collected during two field experiments in 2007. The five MT components were measured at all sites: two horizontal electric and magnetic field components measured in N-S (x axis) and E-W (y axis) directions and the vertical magnetic field component (z axis). The registration time at each site was about 60 h and the periods recorded range from 0.001 to 1000 s. The time series were processed using a standard robust processing algorithm [*Egbert and Booker*, 1986] to obtain the impedance tensor components and the geomagnetic transfer functions (Figure 4). The data were in general of good quality and only some sites were affected by cultural noise. However, some gaps appeared in the estimation of the transfer functions around 5–10 s due to the low natural signal (low solar activity) at the time of data recording.

5.1. Induction Arrows

[25] The induction arrows allow a qualitative recognition of lateral conductivity contrasts. They point away from the high-conductivity zones (in Wiese convention) and have the maximum magnitudes where the gradient of resistivity distribution is highest. Figure 5 shows the real induction arrows at 3 different periods. At medium and long periods, the induction arrows are predominantly N and NNE, excepting some sites where direction appears more scattered. Reversals in the vectors sense reveal a heterogeneous crust with several changes in the horizontal gradient of the resistivity structure.

5.2. Dimensionality Analysis

[26] The dimensionality and preferred strike direction of the profile were studied using two approaches: (1) the multisite/multiperiod analysis [*McNeice and Jones*, 2001] based on the *Groom and Bailey* [1989] tensor decomposition and (2) the phase tensor analysis [*Caldwell et al.*, 2004].

[27] Following the multisite/multiperiod analysis, the strike direction was calculated in a period range for all sites by minimizing the global χ^2 misfit between experimental and theoretical Groom-Bailey impedance tensor. An error floor of 10% was applied to the data because several sites were affected by noise, mainly in the period range between 1 to 10 s; obvious outliers were excluded from the analysis. The results showed that for strike directions between 125° and 145°, the χ^2 error lies within the 95% confidence interval for a period range of 5–200 s. The smallest χ^2 error was achieved for a strike direction of 125°; this value was also confirmed by single site calculations of the strike direction for the same period range. The 90° ambiguity was solved considering the known strike direction of the main geological contacts and the induction vectors (Figure 5).

[28] The phase tensor is defined by the relation $\mathbf{\Phi} = \mathbf{X}^{-1}\mathbf{Y}$, between the real ($\mathbf{X}$) and imaginary $\mathbf{Y}$ part of the impedance tensor, respectively. As any second rank tensor, the phase tensor can be represented graphically as an ellipse, which is defined by 3 invariants of the phase tensor: the principal axes Φ_{max}, Φ_{min}, showing the maximum and minimum phase difference between the magnetic and electric fields and a third coordinate invariant parameter β (the skew angle) that represents the asymmetry of the phase response. The phase tensor is distortion independent, thus in a 2-D case the strike direction can be inferred directly from the orientation of the ellipse. For a 3-D conductivity structure the orientation of the phase tensor ellipses gives the direction of maximum resistivity gradient. The skew angle β provides a measure of the significance of 3-D effects in the MT phase response. Figure 6 shows the phase tensor ellipses of the observed data as a pseudosection. The background color and the color used to fill the ellipses show that β values are low (<5°) but increase to ~10° at long periods (~150 s) and at sites/areas where data quality is lower.

[29] The rose diagrams (Figure 7) show the phase tensor azimuth for different frequency ranges; to exclude the data with strong 3-D effects from the strike analysis only data with $\beta < |4|$ are shown. For short periods, the phase tensor azimuth scatters over a wider range but have a maximum at about 20°–40°, whereas for the period range of 5–200 s a clear maximum at 25–35° exists. For periods > 200 s only few data have low β values. The TM mode data at all sites have been checked for consistency with 1-D D+ models [*Beamish and Travassos*, 1992] and are compatible with a 1-D model except at those sites with high β values. These sites are the responsible for the large error floor required by the multisite/multiperiod analysis to account for a 2-D dimensionality. Therefore, the 2-D approach is expected to be feasible provided a 2-D model error floor large enough to accommodate potential three dimensionality is used.

[30] Thus, in accordance with the results from the multisite/multi–period analysis, and, considering the induction vectors and the known geological strike, a resistivity strike direction of N125°E was chosen. Accordingly, the data were

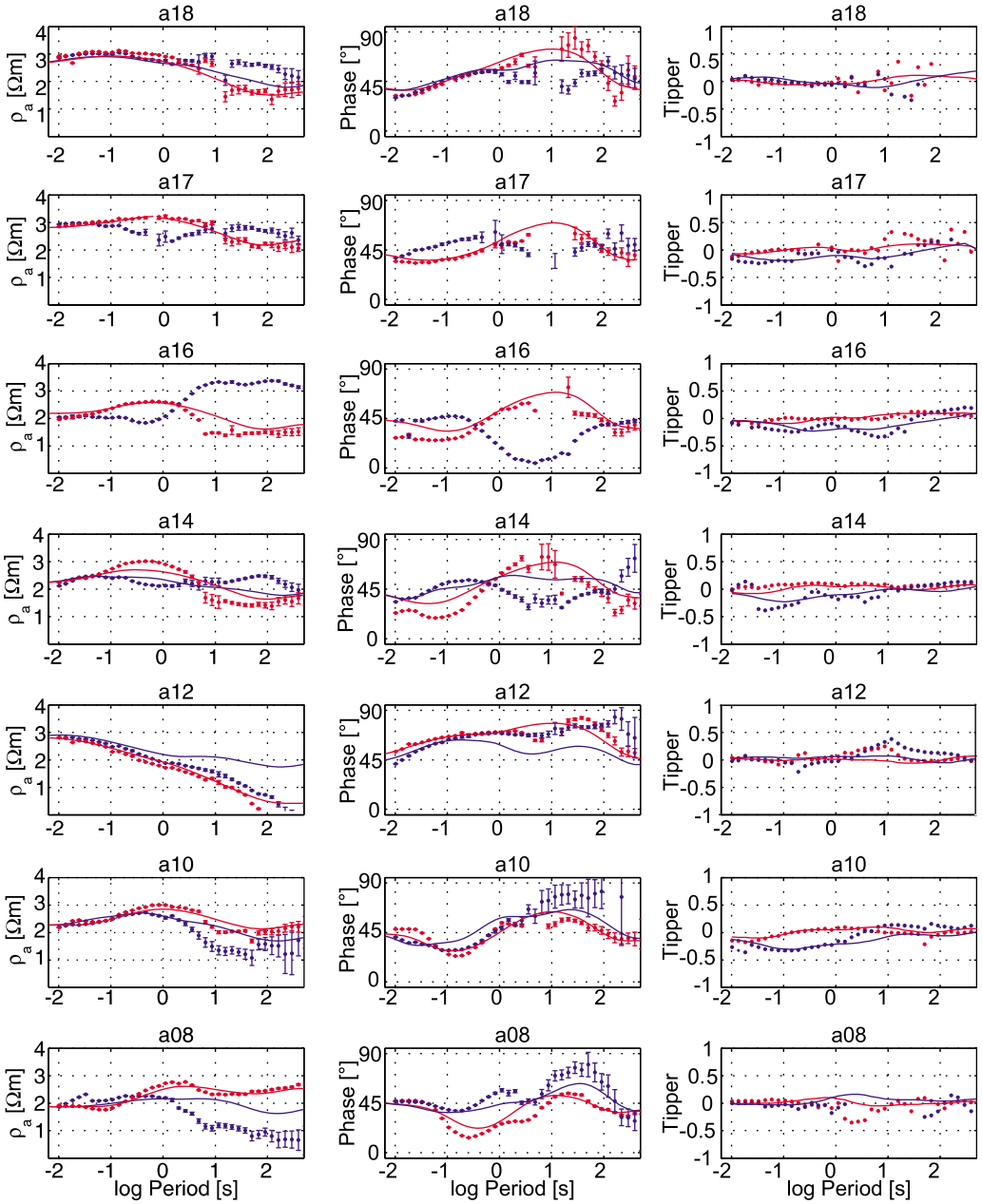

Figure 4. Data and model responses, apparent resistivities, phases (red, TM mode; blue, TE mode), and projected geomagnetic transfer functions (red, imaginary; blue, real).

rotated to −55°, the *xy* component being the TE mode and the *yx* component the TM mode.

5.3. Static Shift and TEM Soundings

[31] In order to control the static galvanic distortion caused by very small scale surface-scattering bodies, a central loop transient EM resistivity (TEM) sounding was made at each MT site to obtain the shallow apparent resistivity. The TEM data were recorded by using the TEM-FAST48HPC equipment (AEMR). It is a small and compact electromagnetic transient source/receiver with 48 time channels and acquisition range from 4 μs to 15.3 ms; soundings were done with a 75 m side coincident single square loop.

[32] Interpretation of the TEM data was carried out using a standard algorithm for 1-D modeling [*Raiche et al.*, 1985]. MT and TEM data can be jointly visualized using semianalytic and empirical relationship [e.g., *Meju*, 1996] establishing that the equivalent MT period (T) for a given transient time (t) in seconds is T ≈ 4t. The shallow resistivity proved to be rather similar to the levels of the (−55° rotated) MT apparent resistivities, whose scattering in the levels was less than one decade. Only few sites showed significant differences between TEM and MT curves; these

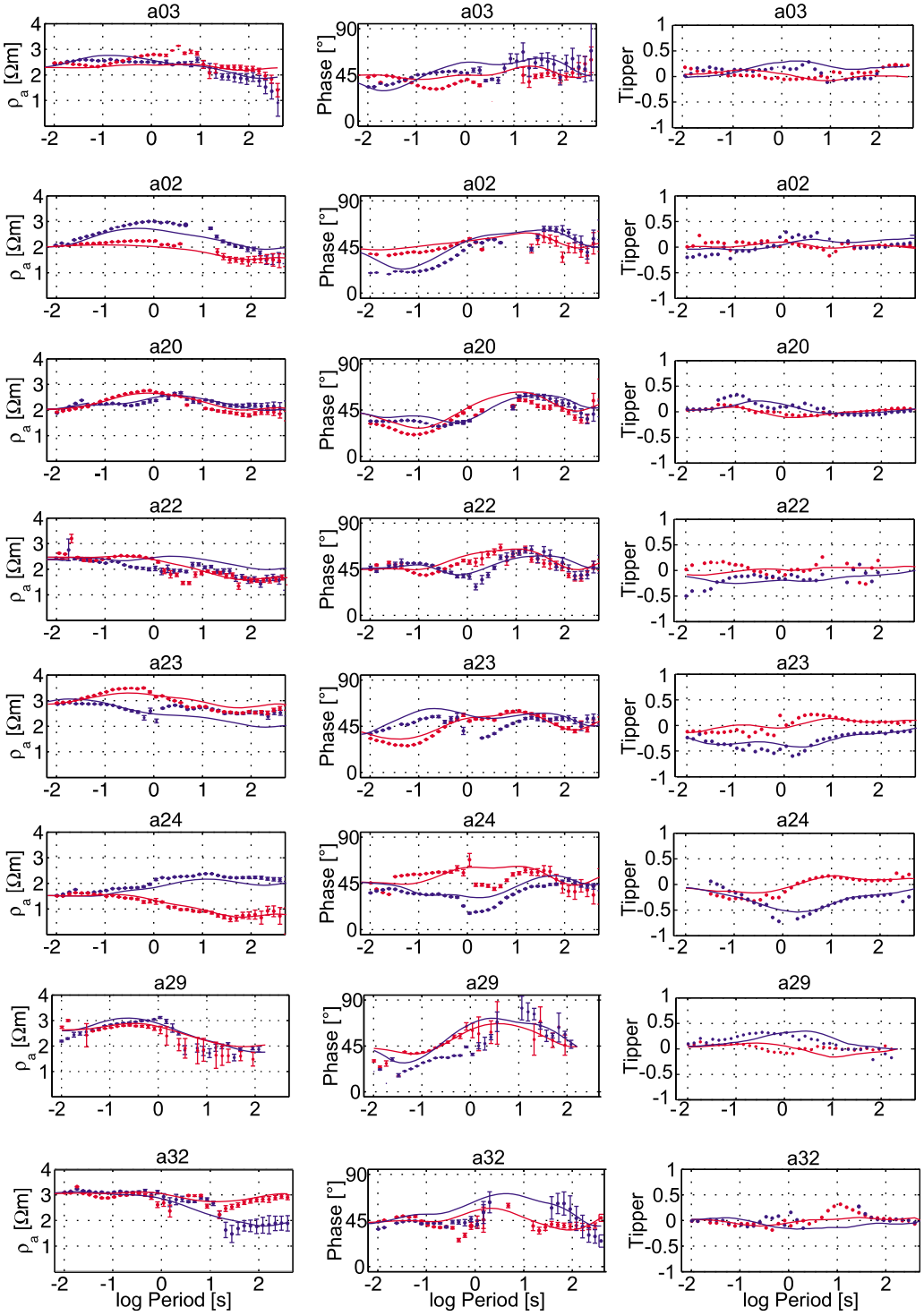

Figure 4. (continued)

apparent resistivities were shifted in accordance with the TEM data *prior* to the inversion. Finally, in the inversion procedure some static shifts were corrected at sites where the fitting did not improve. Figure 8 shows the superposition of TEM data and MT apparent resistivities for two sites; site 24 is an example of good agreement between both TEM and MT data; site 20 illustrates the shift needed to adjust the TEM curve.

5.4. A 2-D Inversion

[33] In accordance with the dimensionality analysis, a joint 2-D inversion [*Rodi and Mackie*, 2001] of −55° rotated

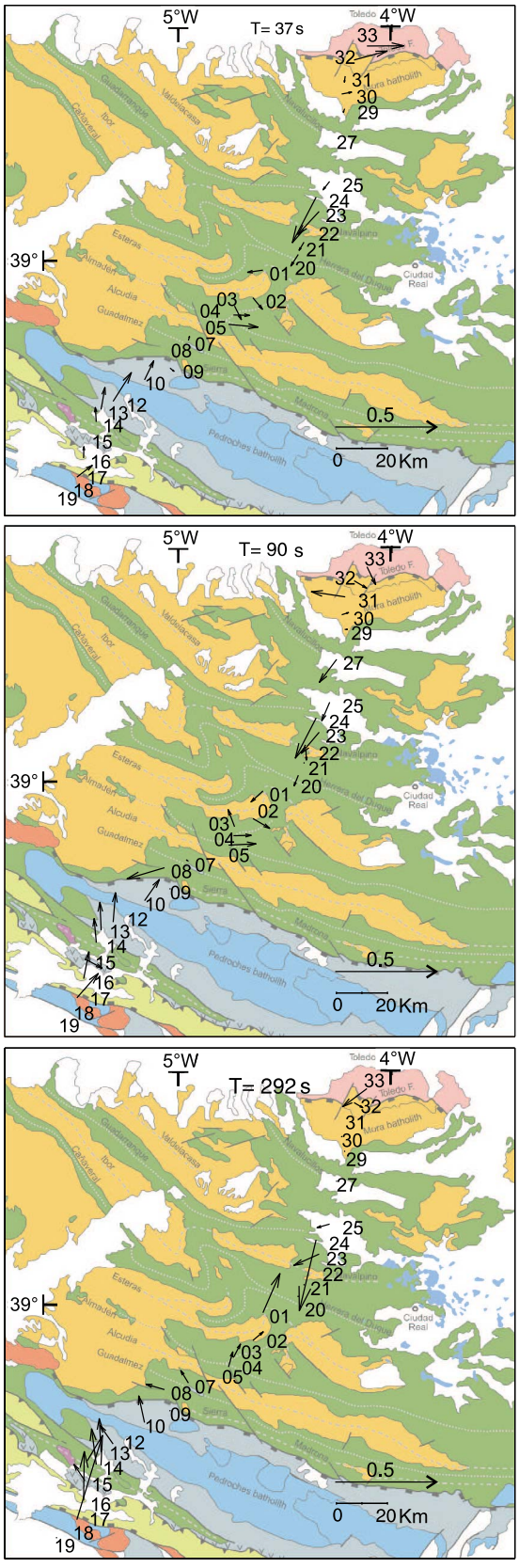

Figure 5. Real induction vectors (Wiese convention, pointing away from conductors) at 37 s, 90 s, and 292 s.

apparent resistivities, phases and projected geomagnetic transfer functions was carried out. The model minimizes second derivatives using equal grid Laplacian and a regularization parameter τ = 7. This value was obtained by optimizing the trade-off between smoothing the model and lowering the RMS misfit (Figure 9). The error floor used in the inversion has to be consistent with the Groom-Bailey dimensionality/strike analysis. The 10% error floor required to establish a 2-D strike direction represents, for the inversion, an error floor of 21% for the apparent resistivities and 5.71% for the phases. A number of inversions were carried out with different errors floors around these values, always obtaining the same relevant features in the final inverse models. In a 2-D Earth, the MT data separate into two independent modes, the TM and TE modes, corresponding to electric current flow perpendicular and parallel to the strike direction, respectively. Since the TE mode is more sensitive to off profile (3-D) structures [*Wannamaker et al.*, 2002], we obtained better fits of the TM mode by slightly reducing the error floor of this TM mode. In addition, the TE mode of those sites, where dimensionality analysis gave a strike removed from the N125°E and data were affected by possible 3-D effects was excluded from the inversion in order to improve the fitting and reduce the rms. These are the sites in the southern part of the profile: sites 15, 16 and 17 in Figure 4. After several attempts the best fitting model was obtained by the following sequence. First, the geomagnetic transfer functions were inverted with a homogeneous Earth starting model. Second, this inverse model result was used as an initial one for the joint inversion of the TM mode and TF data. Finally, the resulting model was used as the starting model for the joint inversion of the TM, TE and TF data. Finally, the model in Figure 3c was obtained with a RMS of 2.96 and an error floor of 21% for the TE apparent resistivities, 15% for the TM apparent resistivities and the same 5.71% for both phase modes. This model is essentially the same obtained when using also the TE mode of the sites 14 to 16 and when using a higher (21%) error floor for the TM apparent resistivities.

[34] Figure 4 shows the model responses for a representative selection of sites, and Figure 10 shows the pseudosections for all the sites along the profile. Figure 10c also contains the difference pseudosections between the observed and modeled responses. The fit is better for the TM mode and tipper whereas the TE mode shows some misfits due to the higher error floor used for this mode. The difference pseudosections show that generally a good fit is achieved for the TM mode. Large misfits, mainly in the TE mode, are found where the data is strongly affected by 3-D structure (e.g., sites 9 and 10), as indicated by the large β values in Figure 6. The main features of the model are constrained mainly by the TM mode. The inverse model obtained from joint inversion of the TM mode and tipper is essentially the same, which gives confidence to the 2-D approach used.

5.5. A 2-D Electrical Resistivity Model

[35] A first view of the electrical resistivity model (Figure 3c) reveals an almost continuous conductive layer along the middle-lower crust (C1 and C2), while the upper crust is imaged as a combination of variably sized resistive and conductive bodies (R1, R2, C3, R3, C4, …, C8). In the

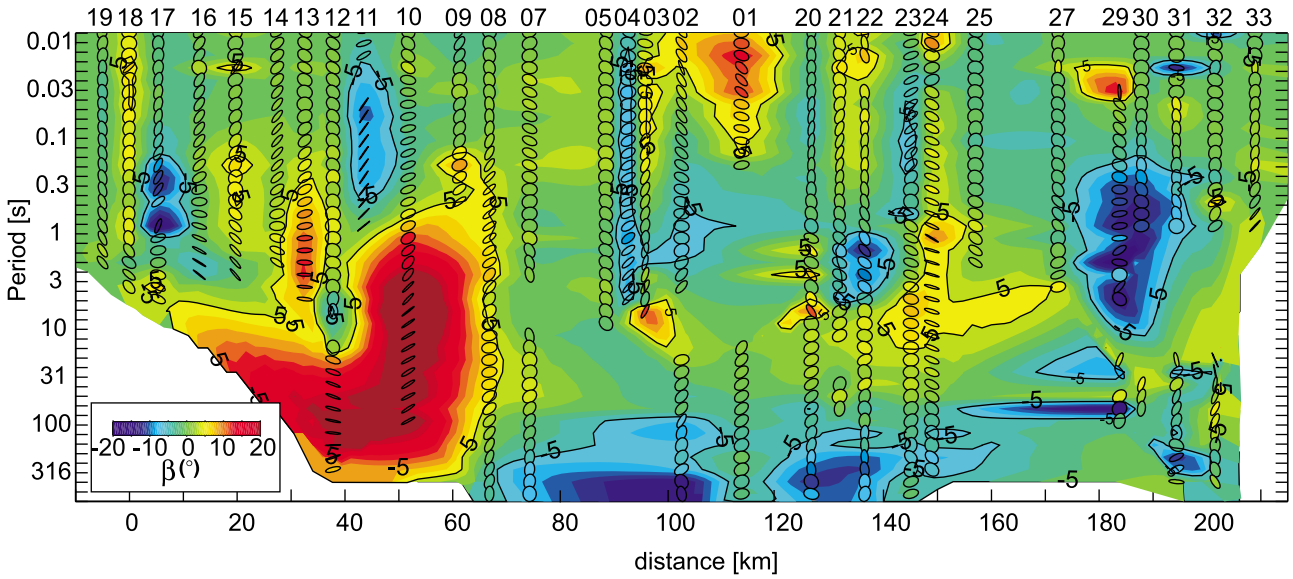

Figure 6. Phase tensor ellipses of the observed data. Ellipses were normalized by Φ_{max}; the background color and the color filling the ellipses show the skew angle β. Orientation of the principal axes of the phase tensor ellipses suggests a N125°E strike direction. High values of β show data affected by 3-D structures; low values of β and uniform orientation of the ellipses suggest that a 2-D modeling approach is justified.

shallow part of the model, some elongated conductors dipping to the north and south coincide with known fault zones and, therefore, the enhanced conductivity is assumed to reflect aqueous fluids trapped in these highly permeable rock domains (including the adjoining fractured rocks). The resistive zones correlate well with igneous intrusions and metamorphic rocks. This shallow part of the model will be described and interpreted in detail in the light of the accurate geological cross section (see section 6.2).

[36] The moderate conductive middle to lower crust, appearing with a dome-like geometry in the north of the OMZ-CIZ boundary and other dominant directions along the model, confirms the prolongation into the CIZ of the conductive layer previously detected in the OMZ [*Muñoz et al.*, 2008]. The absolute electrical conductivity of this layer is fairly homogeneous but enhanced conductivity is observed below sites 7, 10 and 28. At some locations, the upper section of this layer connects with the shallow conductors, imaging a detached and imbricate faulted upper crust.

[37] The joint inversion of apparent resistivities, phases and tipper strongly constrains the model at shallow and middle depths. Given the high error floor used in the inversion a number of acceptable models matching the data could be expected at deeper depths. However, sensitivity

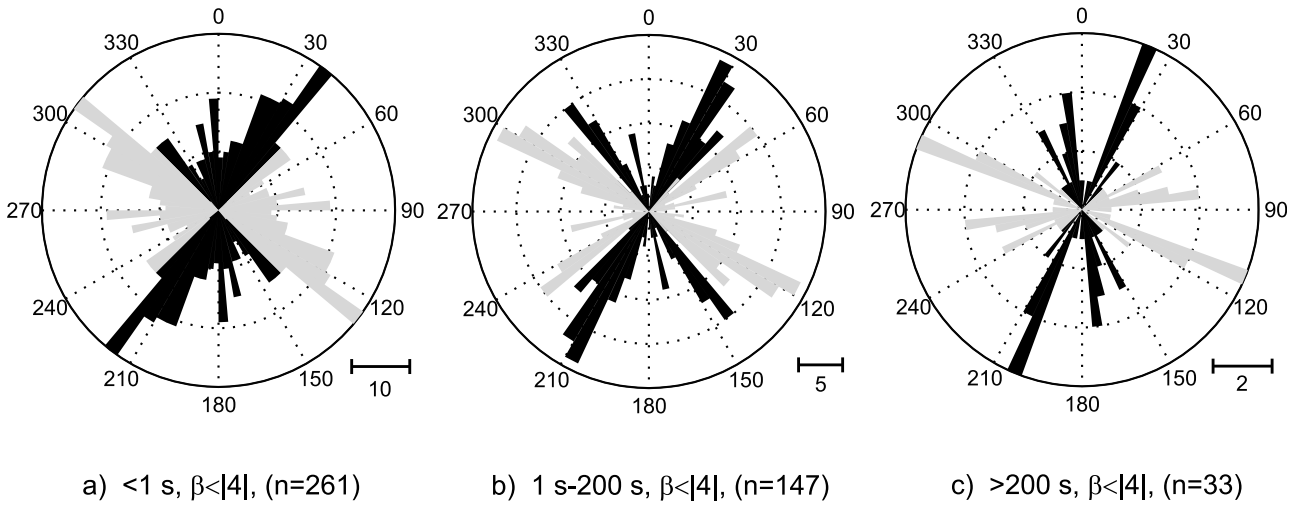

Figure 7. Rose diagrams for the phase tensor azimuth derived from the MT sites at a frequency range of (a) <1 s, (b) 1–200 s, and (c) >200 s. Only data where the skew angle $\beta < |4|$ were taken into account. The ambiguity of 90° is shown by the gray and black roses; n denotes the total number of frequencies.

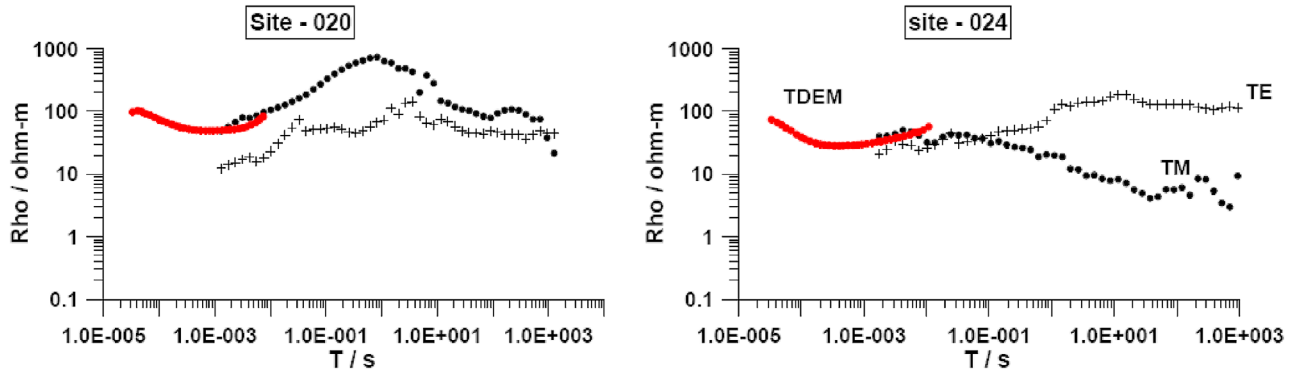

Figure 8. Combined apparent resistivity curves from the TEM (solid line) and the MT soundings for sites 20 and 24.

tests that were carried out by removing the conductors from the model, always resulted in a large data misfit. The resolution decreased only in the deepest parts of the model (>30 km). Specifically, the tests carried out consisted of, first, removing separately each one of the conductors appearing in the model (Figure 11a) and, second, removing the whole conductive middle to lower crust layer corresponding to C2 in the model (Figure 11b). In all the tests the conductors were substituted by a moderate resistivity (300 Ω m) from a depth of 15 km down to 35 km. The largest misfit in all the cases appears in the TM mode, the TE mode being less restrictive. Removing one of the conductors of the final model always resulted in a significant increase of the TM apparent resistivity at middle and long periods in those sites over or near the removed conductor. Note that the resistivity used as a substitute of the conductors in the tests is not high. This indicates that this period range (about 1–100 s) is sensitive to the resistivity structure at midcrustal levels in CIZ. Note also that this period range is within the range where the dimensionality analysis resulted in a 2-D structure. The fitting obtained in this period range (Figure 10) also shows the feasibility of the 2-D approach. Owing to the complexity of the 2-D model, the responses do not depend exclusively on one body since an interaction of all the effects of all the bodies occurs. In the test of Figure 11b where the entire layer C2 in the CIZ is removed the responses of the altered model (green) are similar to those of the models of Figure 11a, the small differences being due to the 2-D effects caused by lateral conductors which are still present in the altered models of Figure 11a. We can conclude that the conductors C1–C9 appearing in the model (Figure 3c) are required by the data and only slight variations in the geometry (depths) are possible.

6. Discussion of the MT Image in the Frame of Geological and Geophysical Data

6.1. Implications of the Middle to Lower Crust Conductive Layer

[38] The IBERSEIS seismic reflection profile [*Simancas et al.*, 2003] imaged in SW Iberia (SPZ, OMZ and southernmost CIZ) a midcrustal detachment shear zone (at 4 to 6 s of depth) where many first-order Variscan structures merge upward to surface. Thus, this shear zone may correspond to the limit between a metasedimentary sequence (the Serie Negra Group and overlying rocks) detached from a high-grade metamorphic/igneous lower crust basement. Dense wide-angle seismic data, partially superposed to the IBERSEIS profile, show relatively high seismic velocities from 4 s to the Moho depth, thus providing evidence of a prevailing mafic composition (mafic granulites with mafic intrusions) for the middle and lower crust in the SPZ, OMZ and southern CIZ (from the Central Unit to the Alcudia Anticline) [*Palomeras et al.*, 2009]. The moderate conductive middle to lower crust should then be attributed to a mafic granulite layer, perhaps bearing interconnected graphite films as proposed by *Monteiro Santos et al.* [2002] and *Muñoz et al.* [2008] for OMZ. The earlier data are in accordance with the conductive middle to lower crustal layer (C1) imaged by MT (Figure 3c). Furthermore, the upper section of C1 can be interpreted as corresponding to the lower part of the Serie Negra Group (SN, Figures 3c and Figure 12), presumably recrystallized under higher metamorphic conditions. Note that the Serie Negra Group has

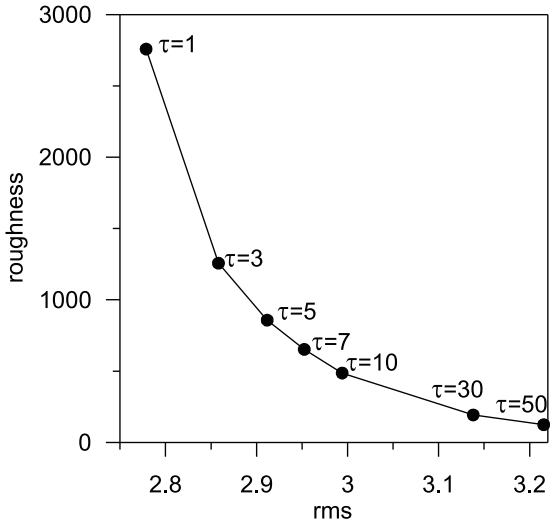

Figure 9. L curve, trade-off between model roughness and root mean square. The optimal parameter τ is 7.

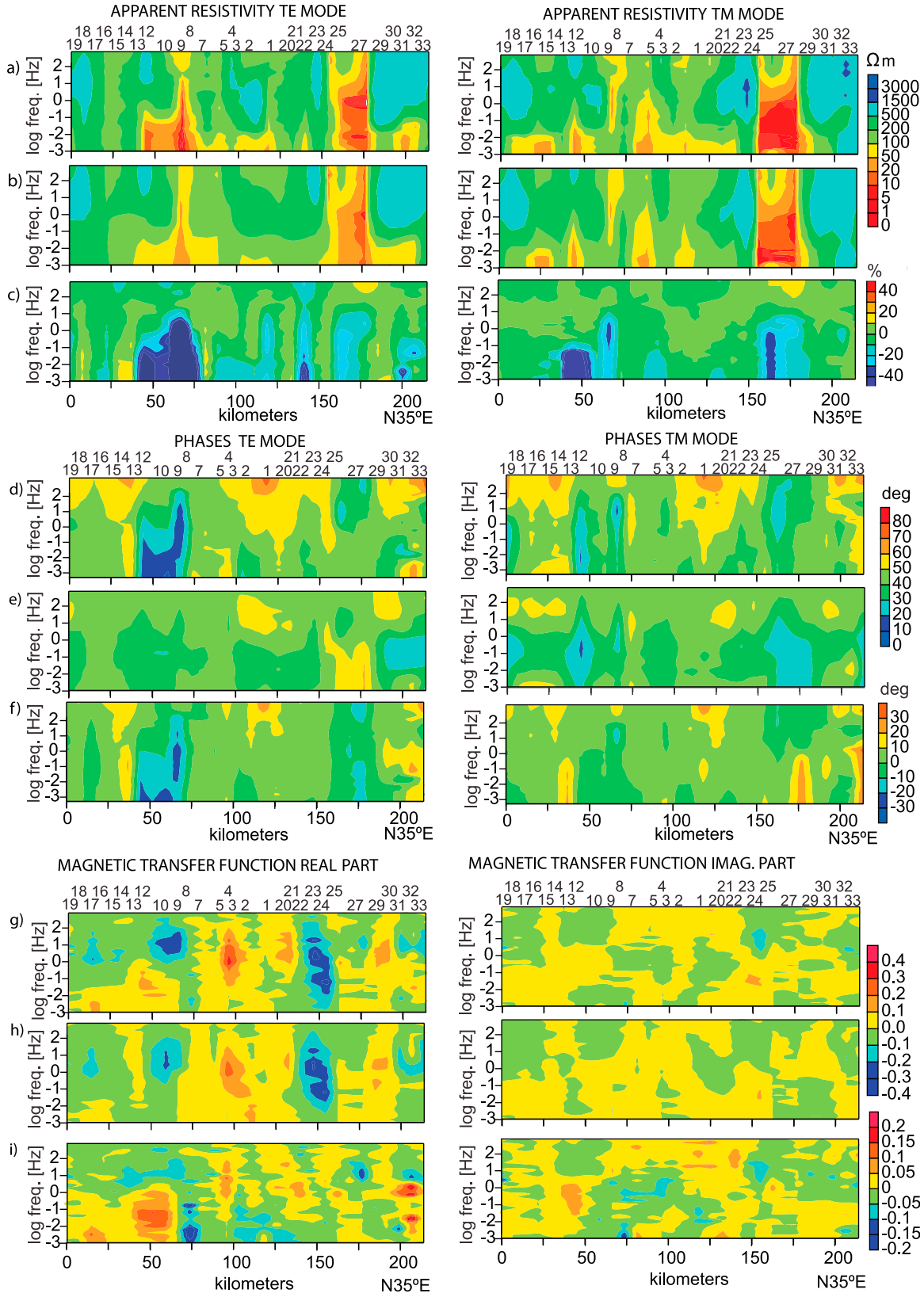

Figure 10. Pseudosections of leveled apparent resistivities, phases, and projected geomagnetic transfer functions. (a, d, and g) data; (b, e, and h) model responses; (c, f, and i) difference between data and model responses.

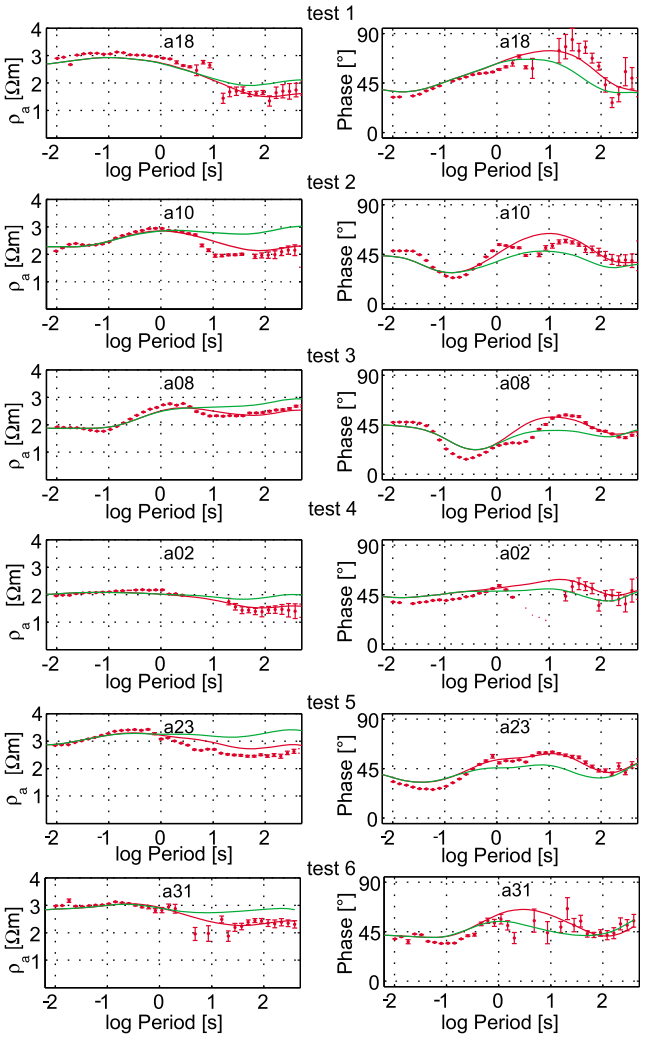

Figure 11a. TM data and model responses for several sensitivity tests. The dots represent the data, the red solid line represents the responses of the inverse model (Figure 3c), and the green solid line represents the responses of the altered models. Replacing the conductors by a resistivity of 300 Ω m, test 1, SN and C1; test 2, C6; test 3, C2; test 4, C2 beneath site 2; test 5, C2 beneath sites 22–23; test 6, C9 and C2 beneath sites 28–31.

proved to be highly conductive because of the presence of interconnected graphite [*Pous et al.*, 2004; *Monteiro Santos et al.*, 2002].

[39] The persistence of a granulitic middle to lower crust to the north of the Pedroches Batholith, as represented by the moderate conductive C2 layer, is not so clear, but other geophysical data contribute to achieve a similar interpretation. A preliminary processed image of the ALCUDIA seismic reflection profile, coincident with our MT profile, shows a persistent very reflective crust from ~5 s to the Moho depth [*Tejero et al.*, 2008]. A ductile banded middle to lower crust formed by alternations of acidic and basic granulites would generate this strong reflectivity and probably be conductive. Contrary to that for the southern part, there are no seismic wave velocity data for the central and northern parts of the profile, in order to constrain its nature. However, the persistence of the same seismic fabric and moderate conductivity both point to middle to lower crust homogeneity all along the profile. Thus, we interpret C2 in a similar way than C1, as corresponding to a middle to lower crust basement formed by banded mafic (and alternating acidic?) granulites. Furthermore, as in the case of C1, the upper section of C2 (e.g., the moderate conductive middle crust between sites 1–4, 6–8, 20–24, or 27–28) could correspond to either (1) the Serie Negra (if it continues below the Alcudian succession northward of the Pedroches area) or (2) to the Alcudian succession itself. In the latter hypothesis, the conductivity of the Alcudian slates has not yet been probed, but it is reasonable to assume the presence of some metamorphosed organic matter, which would account for a fraction of the electrical conductivity imaged, at least in the deepest (and more metamorphosed) Alcudian rocks.

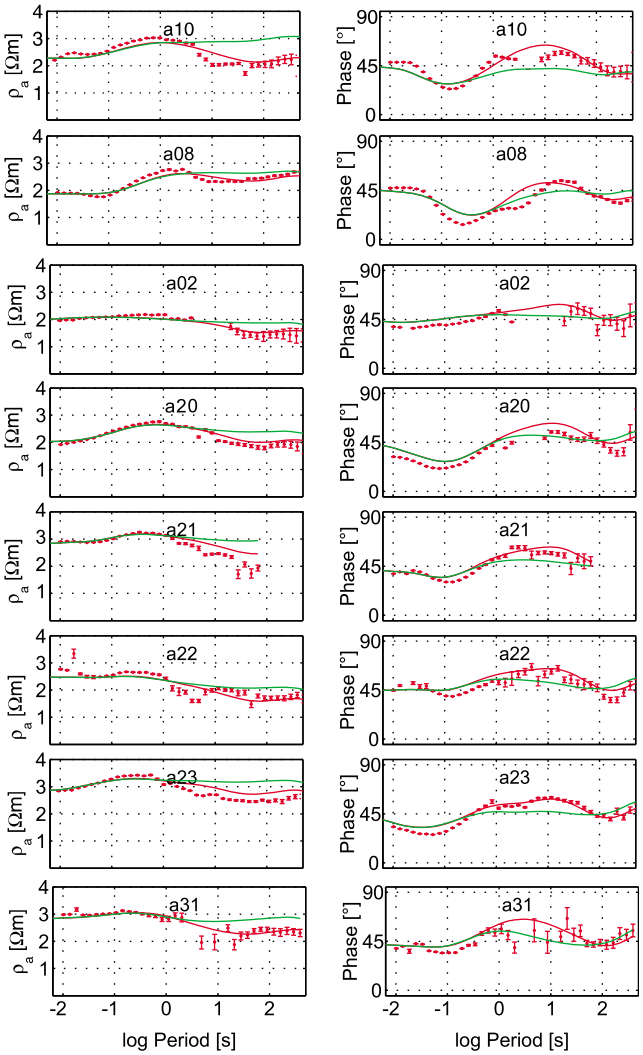

Figure 11b. TM data and model responses for a sensitivity test. The dots represent the data, the red solid line represents the responses of the inverse model (Figure 3c), the green solid line represents the responses of the altered model. The conductive layer in the CIZ middle to lower crust (conductors C2, C6 and C9) is replaced from 15 km down to 35 km by a resistivity of 300 Ω m.

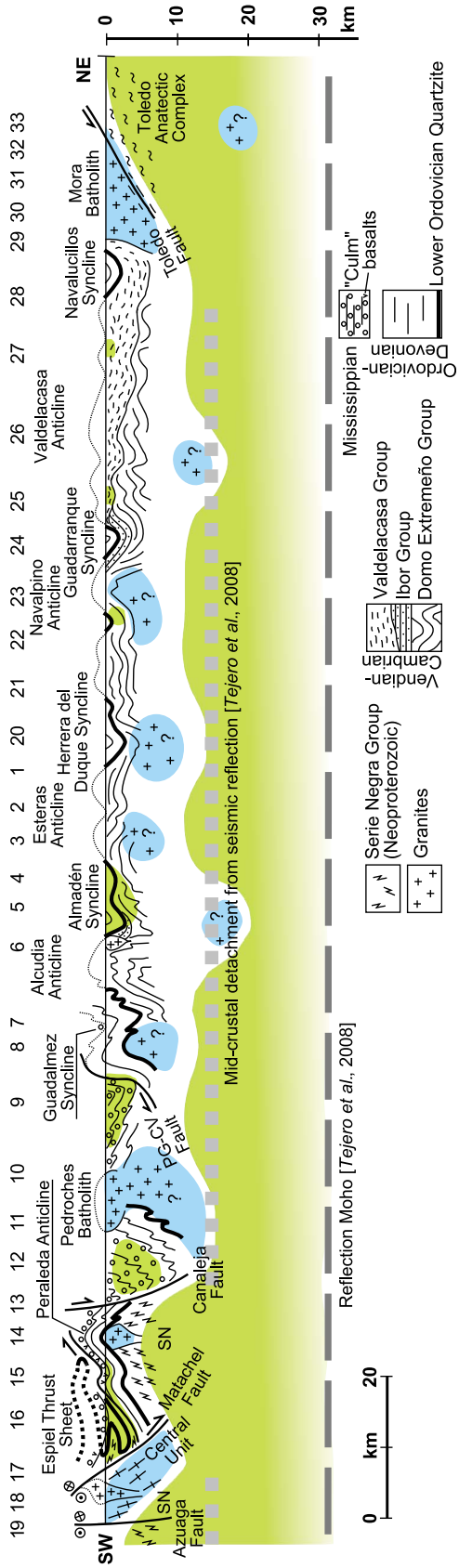

Figure 12. Composite interpretative sketch of the crust including the surface geological cross section (see Figure 3a), the approximate projection of the conductive (green) and resistive (blue) bodies identified along the MT profile (see Figure 3c), the approximate location of the seismic Moho discontinuity (at 10 s TWT depth) and the inferred midcrustal detachment (at 5 s TWT depth) as preliminary imaged by a coincident deep seismic reflection profile [*Tejero et al.*, 2008].

[40] The top of the conductive middle to lower crustal layer (C1 and C2) can represent a major midcrustal décollement, from where the upper crustal structures merge upward to surface (Figure 12); therefore, soft metasediments immediately above the granulite layer should have acted as a décollement horizon. This interpretation is consistent with the general tectonic model reported in the work of *Muñoz et al.* [2008] for the OMZ-CIZ boundary. As for the CIZ concerns, such an interpretation is constrained by the following joined arguments. (1) Somewhere in the middle crust there must be a first-order rheological contrast derived from a petrological one: the lower crust is likewise interpreted as a mafic granulite crystalline basement, and the upper crust is formed by thick metasedimentary successions intruded by granites. (2) This compositional contrast is corroborated by a relevant midcrustal jump in seismic wave velocities for the southern CIZ (from the Central Unit to the Alcudia Anticline) [*Palomeras et al.*, 2009]. (3) The middle to lower crust has been preliminary seismically imaged as homogeneous and highly reflective (then interpreted as ductile banded), while the upper crust is rather transparent [*Tejero et al.*, 2008]. (4) Our MT data image a middle to lower crust electrically homogeneous and moderately conductive, in contrast with the alternating conductive and resistive bodies for the upper crust. (5) From the structural point of view, the lower crust seems to be quite homogeneous (as suggested from its electrical and seismic character); on the contrary, the uppermost crust is tectonically deformed by a train of upright folds and faults (Figure 3a) that do not seem to penetrate into the lower crust or mantle. Consequently, the tectonic structures of the upper crust should be detached and rooted in a midcrustal décollement (Figure 12), in a similar way than for the SPZ, OMZ and southernmost CIZ was imaged by the IBERSEIS seismic profile [*Simancas et al.*, 2003]. The only difference is that in the OMZ (and partially in the southernmost CIZ), the Iberseis Reflective Body is superposed to the midcrustal detachment. The existence of this geophysical body (associated with both high electrical conductivity and high and complex seismic reflectivity) has been explained as the result of a mantle thermal pulse that resulted in abundant mafic magmatism during an intracollisional Mississippian extensional event [*Simancas et al.*, 2003]. The northern evidence of this extension is the Mississippian Pedroches Basin and related basalts. Further to the north there is no Iberseis Reflective Body (therefore, the middle crust in the CIZ is not as so conductive as in the OMZ), nor Mississippian (thick) sediments or mafic igneous. But the absence of the Iberseis Reflective Body (and its related features including enhanced conductivity) to the north of the Pedroches area does not mean an absence of a tectonic detachment between the upper and lower crusts.

[41] The continuity of this regional midcrustal décollement is vertically displaced at least below four locations: beneath site 13 (northward of the OMZ-CIZ boundary) the displacement is responsible for the dome-like geometry of the conductive layer in the southern part of the model; beneath site 9, site 24 and, toward NE, site 33, the tectonic disruption appears to be less important, despite causing a rough waving pattern of that crustal layer. The enhanced conductivity in some of these structural discontinuities could be ascribed to an increase in the graphite content/interconnectivity as a result of (1) hydrothermal circulation of C-rich fluids during the overall transpressive Variscan regime and/or (2) shearing of graphite-rich rocks belonging to the Serie Negra (as seems to occur beneath sites 9 and 13). The shallow character of the conductive signal in other areas may be due to a combination of tectonic effects and mineralogical characteristics of some metasedimentary horizons, and the very fact that metamorphosed sequences are strongly affected by Variscan deformation (folding) may also reinforce locally this pattern (e.g., Almadén syncline).

6.2. A Closer View of the Upper Crust: A Comparison With the Geological Cross Section

[42] The detailed geological cross section along this MT profile provides an opportunity to check the usefulness of the MT method to image the shallow structure of the crust. Resistivity changes in the upper crust are usually ascribed to the presence of aqueous (saline) fluids and/or mineral conductive phases rather than to changes in lithological features. But similar rocks recording variable effective (interstitial) porosity and (fracture) permeability, and eventually subtle differences in proportion to their forming conductive minerals can also account for marked differences in electrical resistivity values. In line with this rationale, the MT features of the upper crust and their possible connections with deeper structures or rock bodies will be investigated.

[43] The profile starts in the south with R1, but its meaning is somewhat imprecise because of the marginal location in the model. R2 is a north dipping resistive domain that coincides with the Central Unit (from sites 19 to 17), where resistive rocks (gneisses and amphibolites) prevail; the Late Variscan granite intruding into the Central Unit between sites 18 and 17 also contributes to this resistive signal. R2 disappears downdip to the north into the middle to lower crustal conductive layer. All these features are in accordance with the geometry imaged for the Central Unit by the IBERSEIS profile [*Simancas et al.*, 2003]. Between the vertical trace of the Azuaga Fault and R2, a conductive triangle-shaped domain (Figure 3c) is interpreted as the continuation of the Serie Negra to the north of this fault zone, underlying the Central Unit and reinforcing the paleogeographical continuity between the OMZ and CIZ during the Neoproterozoic. This conductor, just beneath (few kilometer depth) of the boundary OMZ-CIZ, appears in all the MT profiles carried out in SW Iberia and has been interpreted as the signature of this suture at depth, the graphite being responsible for the high conductivity [*Pous et al.*, 2004; *Muñoz et al.*, 2008; *Almeida et al.*, 2005].

[44] C3 is a shallow (0 to 5 km of depth) conductive body located between sites 17 and 15, and fits well with the characteristics displayed by the outcropping rocks and their structural arrangement. Here, the Espiel Thrust Sheet (an allochthonous unit bounded by the Matachel Fault and the Espiel Thrust to the south and north, respectively) develops a recumbent folded structure that involves, among others, metamorphosed rocks of the Serie Negra (outcropping between sites 17 and 16). In addition, just to the north of the Espiel Thrust, around site 15, Mississippian metabasalts and minor slates (which must also be conductive, see below) crop out along the southern limb of the Peraleda Anticline. There is just one site (16) within this profile segment, but

the good resolution of the geological cross section supports fairly well this interpretation. Note, however, that the lateral waveshape of the electromagnetic field leads to a significant contribution of sites 15 and 17 in constraining C3.

[45] Between the Azuaga Fault and the Peraleda Anticline, there are several igneous bodies, some of which host ore-forming systems or trigger their development in the metamorphic envelope, thus accounting for the observed magnetic anomalies (Figure 3b).

[46] The MT features in the Peraleda Anticline, with its fold axis centered at site 14, are interesting for two reasons. First, the position of Perelada Anticline coincides with the minimum depth of the conductive C1 (overlying Serie Negra) layer, thus drawing an antiformal geometry; metamorphosed rocks of the Serie Negra constitute the core of the anticline and, in fact, they outcrop below Lower Paleozoic metasandstones 15 km to the northwest of site 14 (Figure 2). Second, the MT profile lies across the Peraleda Anticline just where erosion of the unconformable overlying Lower Paleozoic sandstones allows the Valsequillo stock to outcrop. The Valsequillo stock corresponds to a Neoproterozoic granite intruding into the Malcocinado Formation, here represented by volcanogenic metaconglomerates over the Serie Negra. The R3 body fits very well with this shallow granite located in the Peraleda Anticline core.

[47] Below site 13, the conductive layer C1 is suddenly displaced down to lower crustal depths. At surface, the northern limb of the Peraleda Anticline is disrupted by the Canaleja Fault, which downthrows the northern block (Figure 3). Dip slip of this subvertical fault has been estimated, from balanced cross sections, at a minimum of 5000 m, although it could be higher [*Martínez Poyatos*, 2002].

[48] C4 and C5 conductive bodies are located just below sites 12 and 9, respectively, and centered in the "Culm" facies (Mississippian rocks) bounding the Pedroches Batholith (Figure 3). The Mississippian succession is here dominated by a monotonous interchange of dark slates and metagraywackes. By sectors, the slates are the unique rock type and their dark shade could be due to significant enrichments in metamorphosed sedimentary organic matter (as in the Serie Negra metasediments with high graphite content); nonetheless, the intensity of metamorphism in the Pedroches area did not exceed very low grade conditions (200°C–300°C [*Martínez Poyatos et al.*, 2001b]).

[49] In addition to the previous interpretation, C5 can also be due to features triggered by active faulting through time. In fact, the northern portion of C5 coincides with the PG-CV Fault (located between sites 9 and 8), whose characteristics and relevance [*Martín Parra et al.*, 2006] should now be considered. At surface, the fault dips to the south and separates the Mississippian succession from the underlying Paleozoic rocks located to the north. Along most of its trace, the fault sheared a well-known graphite-rich, 100 m thick, Silurian shale. Also common is the record of effects due to a long-lived hydrothermal system, involving various fluid pulses focused under distinct (P-)T conditions: (1) synshearing to postshearing porphyroblasts of andalusite, biotite, and pyrophyllite (that can reach up to 80 vol % of the phyllonites adjoining granites), even removed from igneous intrusions; (2) abundant kaolinite (rarely present out of the fault zone), muscovite, andalusite, and quartz in phyllonitized shales and clay gouges along the eastern fault segment; and (3) intense kaolinitization and concomitant Pb sulphide ore formation, requiring high volumes of mineralizing fluids at estimated temperatures of 100°C–200°C [*Jiménez-Millán et al.*, 2007]. All these features together with a highly effective permeability (caused by recurrent fracturing and the infiltration of substantial meteoric-derived waters) account for the enhanced conductivity along the PG-CV Fault.

[50] At a regional scale, the PG-CV Fault has been interpreted as the boundary of two crustal domains with some differences in Precambrian and Paleozoic successions, basement compositions (inferred on the basis of isotope geochemistry for granite rocks) and Variscan structures [*Martín Parra et al.*, 2006]. The high conductivity of this structure and its regional relevance suggest a deeper prolongation for the PG-CV Fault, reaching the middle or even the lower crust, as imaged by the south dipping C6 body. Thus, the extreme conductivity of C6 can be ascribed to the shearing undergone by the Serie Negra as it intersects the fault zone at a midcrustal depth, leading to an increase in the content and connectivity of graphite.

[51] As regards the resistive bodies R4 to R12, it should be noted that they are mainly located in the upper crust and are rounded in shape. R4 and R11 underlie the Pedroches (sites 11 to 10) and Mora (sites 29 to 32) granitic batholiths, respectively, also showing negative gravity anomalies (Figure 3b). The assignment of R5, R6, R7, R8, R9, R10 and R12 to subsurface granite bodies is not so straightforward given the absence of significant regional negative gravity anomalies and the near absence of granite outcrops between Pedroches and Mora. Nevertheless, the presence of two very small granite stocks (15 km to the northwest and 30 km to the east of Almadén, respectively; Figure 2) may be taken as evidence for more subsuperficial igneous bodies in the surveyed region.

[52] As for the shape of the Pedroches igneous body, there is evidence to suggest a relevant vertical dimension (deep root), i.e., the existence of an important negative gravity anomaly (up to 20 mGal), the high-dipping contacts with the country rocks, the absence of roof pendants or of large country rock inclusions at some distance from the contacts, and the shape of R4 (exhibiting high resistivity down to 15 km depth). Therefore, in the absence of more detailed gravity data, the interpretation by *Aranguren et al.* [1997] as a thin laccolith intrusion must be treated with caution.

[53] C7 is an upper crustal conductive body located between sites 6 and 5, where the Silurian to Devonian sedimentary succession crops out in the core of the Almadén Syncline (Figure 3). This succession includes, only in the Almadén area, variable types of basaltic rocks hosting Ca-Mg-Fe carbonates, pyrite and cinnabar mineralization [*Higueras et al.*, 2000], which account for the observed conductivity and magnetic anomaly (Figure 3b).

[54] At the northern edge of the MT profile, the upper crust is imaged as a conductive body (C8) matching the Toledo Anatectic Complex (Figure 3). This complex is separated from the Mora Batholith (and its country rocks that crop out at site 32) by the Toledo Fault, located just to the south of site 33. The boundary between C8 and R11 is in accordance with the low dip to the south of the Toledo Fault

[*Hernández Enrile*, 1991]. The dominant lithologies of the Toledo Anatectic Complex are a priori resistive rocks: pelitic migmatites and related granitoids (formed by fast partial melting of the crust under temperature conditions of ~800°C [*Barbero*, 1995]), with minor gabbros. However, the gabbros and some granite facies contain disseminated oxides and Fe sulphides as accessory phases, as occurs in other gneissic domes, that should account for the observed conductivity.

[55] Given the south dip and extensional slip of the Toledo Fault, it is possible to put forward a hypothesis about the roots of the thermal doming that sustained the genesis of the shallow migmatites/granitoids. These roots may be related to a southern and deeper crustal area as imaged by the very conductive C9 body. In this case, a mafic (conductive) granulitic/gabbroic body should have remained here as the nonmelted fraction residue, and it could contain appropriate mineral phases (sulphide?) to contribute to its high conductivity. Note that the depth of C9 is compatible with the maximum retrograde metamorphic pressure recorded in the migmatites (5 kbar [*Barbero*, 1995]). The presence of this rigid body may generate rheological contrasts that are enough to control the geometry of the deeper segment of the Toledo Fault, whose propagation and reactivation may also, be accompanied by active (and focalized) circulation of hydrothermal fluids able to promote the development of deep-seated (sulphide?) mineralization. Accordingly, it would be tempting to connect the Toledo Fault with C9 at depth, although this possibility is geologically unrealistic. The Toledo Fault has a dip of 30° at surface, and due to its extensional regime, toward the south it most probably becomes to a lesser dip or even subhorizontal, as most low-angle extensional faults do at depth. As for the magnetic anomaly observed at that part of the profile, its short-wavelength points to a shallow source in a local feature above R11. The magnetic anomaly is centered at site 29, where it is known the existence of well formed magnetite crystals, together with limonite and haematite mineralizations hosted in limestones that bound the Mora Batholith by the south.

[56] The magnetic anomaly that exists between sites 21 to 24 reaches a maximum of 80 nT, suggesting the presence of a hidden mineralized body that coincides with the shallow conductor C12. This mineralization, presumably quite rich in magnetite ± sulphides may be syngenetic in relation to the Ordovician-Devonian silicicastic sequence (as is well known in many other CIZ sectors) or epigenetic (skarn type) and therefore associated with the postemplacement evolution of the subsurface igneous batholith imaged by R9. In addition, the possible existence of deeper-seated mineralizations (imaged by the moderate conductive middle crust between sites 20 to 24) could also contribute to the observed magnetic anomaly. Furthermore, the moderate conductive character of the middle crust (as represented by the upper section of C2 in those sectors not disrupted by resistive granites) can be also due, as proposed above (see section 6.1), to the existence of interconnected graphite in either the Serie Negra Group (below the Alcudian succession) or in the deeper sections of the Alcudian succession itself.

[57] Finally, small and very shallow conductive bodies are imaged just below sites 27 (C10) and 25 (C11). Both sites are located on large outcrops of recent sediments (Figure 2) deposited in alluvial slopes and valleys surrounding quartzitic ridges. They are composed of quartzitic pebbles embedded in a ferruginous fine-grained matrix that most probably behaves as an aquifer. Such characteristics account for the high conductivity.

7. Conclusion

[58] The new electrical resistivity model obtained from the MT data yields fresh insights into the characterization of the crustal nature and architecture in the CIZ, an internal domain of the Variscan Orogen in SW Europe. Although the data are partly affected by 3-D structures, the extensive strike analysis using the established multisite/multi frequency decomposition of *McNeice and Jones* [2001] and the new phase tensor method [*Caldwell et al.*, 2004] gave similar and reasonable results of a 2-D electrical resistivity structure. The strike direction matches the geological observations and is also confirmed by the direction of the induction arrows, thus indicating that the MT data could be successfully modeled with a 2-D algorithm. However, a careful selection of the data, discarding the TE mode for some sites which are affected by 3-D structures, was necessary to achieve a 2-D resistivity model with a satisfying data fit. Sensitivity tests assure the reliability of the main conductive features appearing in the model.

[59] The structure provided by the MT imaging compared with the detailed geological information and complemented with other geophysical data led to a comprehensive interpretation of the crustal conductivities. In the upper crust, the OMZ-CIZ suture is viewed as a NE dipping (in accordance with seismic data [*Simancas et al.*, 2003]) resistive body surrounded by conductive domains matching sections of the Serie Negra Group. Relevant faults (Matachel, Canaleja, Puente Génave–Castelo de Vide, or Toledo) are conductive zones or coincide with boundaries of high resistivity contrast. Crustal domains including mafic/intermediate rocks that are mineralized or control the development of epigenetic ore systems have magnetic anomalies and are imaged as conductive bodies (e.g., Espiel and Almadén areas). The Mississippian "Culm facies" sedimentary rocks of the Pedroches Basin behave as conductors probably related to graphite content. All the outcropping granites along the studied section are resistive, especially the Pedroches and Mora batholiths, which also show negative Bouguer anomalies. Furthermore, other resistive portions of the upper crust suggest the existence of several hidden igneous bodies in the eastern part of the Schist-Graywacke Complex Domain of the CIZ, some of them being potentially associated with shallow magnetite/sulphide-rich ores.

[60] A relevant result is the existence of a mild but persistent conductive middle to lower crustal body all along the modeled section, interpreted as corresponding to a mafic granulitic basement. This confirms for the first time the prolongation into the CIZ of the conductive middle to lower crust detected in earlier studies along the whole OMZ [*Muñoz et al.*, 2008]. The dome-like geometry of this layer at the OMZ-CIZ boundary and other dominant directions connecting the upper section of the layer with shallow conductors suggest the existence of a main midcrust dé-

collement also in the CIZ, in agreement with *Simancas et al.* [2003] and *Muñoz et al.* [2008] in the OMZ. Thus, the crustal structure in the studied section of the CIZ, as a result of the Variscan orogeny, is similar to other sectors of the belt. In the OMZ and southern CIZ, the upper section of this conductive layer is made up, among others, of the graphite-bearing Neoproterozoic Serie Negra Group, highly sheared and metamorphosed at midcrustal levels. Jointly, all these features point to a similar basement in the most internal domains of the orogen (CIZ and OMZ). From the foregoing account, it follows that these crustal domains were deeply modified and homogenized by the intense tectonothermal Variscan imprint.

[61] **Acknowledgments.** We thank the Spanish Ministry of Science and Innovation for support through grants CGL2006-12259, CGL2007-63101/BTE, CGL2009-07721, TOPO-IBERIA CONSOLIDER-INGENIO CSD2006-00041, and RNM-148. We thank three anonymous reviewers and the Associate Editor for their helpful comments which contributed to clarify the ideas presented in this paper, and they are deeply acknowledged.

References

Almeida, E. P., J. Pous, F. A. Monteiro Santos, P. Fonseca, A. Marcuello, P. Queralt, R. Nolasco, and L. A. Mendez Victor (2001), Electromagnetic imaging of a transpressional tectonics in SW Iberia, *Geophys. Res. Lett.*, *28*, 439–442, doi:10.1029/2000GL012037.

Almeida, E., F. Monteiro Santos, A. Mateus, W. Heise, and J. Pous (2005), Magnetotelluric measurements in SW Iberia: New data for the Variscan crustal structures analyses, *Geophys. Res. Lett.*, *32*, L08312, doi:10.1029/2005GL022596.

Aranguren, A., F. J. Larrea, M. Carracedo, J. Cuevas, and J. M. Tubía (1997), The Los Pedroches Batholith (southern Spain): Polyphase interplay between shear zones in transtension and settings of granites, in *Granite: From Segregations of Melts to Emplacement Fabrics*, edited by J. L. Bouchez, D. H. W. Hutton, and W. E. Stephens, pp. 215–231, Kluwer Acad., New York.

Ardizone, J., J. Mezcua, and I. Socias (1989), Mapa aeromagnético de España peninsular, Inst. Geogr. Nac., Madrid.

Azor, A., F. González Lodeiro, and J. F. Simancas (1994), Tectonic evolution of the boundary between the Central Iberian and Ossa-Morena zones (Variscan Belt, SW Spain), *Tectonics*, *13*, 45–61, doi:10.1029/93TC02724.

Banda, E., E. Suriñach, A. Aparicio, J. Sierra, and E. Ruiz De La Parte (1981), Crust and upper mantle structure of the central Iberian Meseta (Spain), *Geophys. J. R. Astron. Soc.*, *67*, 779–789, doi:10.1111/j.1365-246X.1981.tb06954.x.

Barbero, L. (1995), Granulite-facies metamorphism in the Anatectic Complex of Toledo, Spain: Late Hercynian evolution by crustal extension, *J. Geol. Soc.*, *152*, 365–382, doi:10.1144/gsjgs.152.2.0365.

Beamish, D., and J. M. Travassos (1992), The use of the D^+ solution in magnetotelluric interpretation, *J. Appl. Geophys.*, *29*, 1–19, doi:10.1016/0926-9851(92)90009-A.

Brasse, H., and D. Eydam (2008), Electrical conductivity beneath the Bolivian Orocline and its relation to subduction processes at the South American continental margin, *J. Geophys. Res.*, *113*, B07109, doi:10.1029/2007JB005142.

Burg, J. P., M. Iglesias, P. Laurent, P. Matte, and A. Ribeiro (1981), Variscan intracontinental deformation: The Coimbra-Córdoba Shear Zone (SW Iberian Peninsula), *Tectonophysics*, *78*, 161–177, doi:10.1016/0040-1951(81)90012-3.

Caldwell, T. G., H. M. Bibby, and C. Brown (2004), The magnetotelluric phase tensor, *Geophys. J. Int.*, *158*, 457–469, doi:10.1111/j.1365-246X.2004.02281.x.

Carbonell, R., F. Simancas, C. Juhlin, J. Pous, A. Pérez-Estaún, F. González-Lodeiro, G. Muñoz, W. Heise, and P. Ayarza (2004), Geophysical evidence of a mantle derived intrusion in SW Iberia, *Geophys. Res. Lett.*, *31*, L11601, doi:10.1029/2004GL019684.

Egbert, G., and J. R. Booker (1986), Robust estimation of geomagnetic transfer functions, *Geophys. J. R. Astron. Soc.*, *87*, 173–194, doi:10.1111/j.1365-246X.1986.tb04552.x.

Figueiras, J., A. Mateus, M. Gonçalves, J. Waernborg, and P. E. Fonseca (2002), Geodynamic evolution of the South Variscan Iberian Suture as recorded by mineral transformations, *Geodin. Acta*, *15*, 45–61, doi:10.1016/S0985-3111(01)01078-6.

Franke, W. (2000), The mid-European segment of the Variscides: Tectonostratigraphic units, terrane boundaries and plate tectonic evolution, in *Orogenic Processes: Quantification and Modelling in the Variscan Belt*, edited by W. Franke et al., *Geol. Soc. Spec. Publ.*, 179, 35–61, doi:10.1144/GSL.SP.2000.179.01.05.

Gómez-Pugnaire, M. T., A. Azor, J. M. Fernández Soler, and V. López Sánchez-Vizcaíno (2003), The amphibolites from the Ossa-Morena/Central Iberian Variscan suture (southwestern Iberian Massif): Geochemistry and tectonic interpretation, *Lithos*, *68*, 23–42, doi:10.1016/S0024-4937(03)00018-5.

Groom, R. W., and R. Bailey (1989), Decomposition of magnetotelluric impedance tensor in the presence of local three-dimensional galvanic distortion, *J. Geophys. Res.*, *94*, 1913–1925, doi:10.1029/JB094iB02p01913.

Harinarayana, T., K. Naganjaneyulu, and B. P. K. Patro (2006), Detection of a collision zone in south Indian shield region from magnetotelluric studies, *Gondwana Res.*, *10*, 48–56, doi:10.1016/j.gr.2005.12.006.

Hernández Enrile, J. L. (1991), Extensional tectonics of the Toledo ductile-brittle shear zone, central Iberian Massif, *Tectonophysics*, *191*, 311–324, doi:10.1016/0040-1951(91)90064-Y.

Higueras, P., R. Oyarzun, J. Munhá, and D. Morata (2000), The Almadén mercury metallogenic cluster (Ciudad Real, Spain): Alkaline magmatism leading to mineralization processes at an intraplate tectonic setting, *Rev. Soc. Geol. Esp.*, *13*, 105–119.

Instituto Geográfico Nacional (IGN) (1976), Mapa de España de anomalía de Bouguer, scale 1:1,000,000, Madrid.

Jiménez-Millán, J., N. Velilla, and M. Vázquez (2007), Two-stage formation of kaolinite in shear-zone slates, southern Iberian Massif, SE Spain, *Clay Miner.*, *42*, 273–286, doi:10.1180/claymin.2007.042.3.01.

Jones, A., I. Ferguson, A. Chave, R. Evans, and G. McNeice (2001), Electric lithosphere of the Slave craton, *Geology*, *29*, 423–426, doi:10.1130/0091-7613(2001)029<0423:ELOTSC>2.0.CO;2.

Julivert, M., J. M. Fontboté, A. Ribeiro, and L. E. Nabais Conde (1972), Mapa y memoria explicativa del mapa tectónico de la Península Ibérica y Baleares a escala 1:1.000.000, 113 pp., Inst. Geol. Min. Esp., Madrid.

Lahti, I., T. Korja, P. Kaikkonen, K. Vaittinen, and the BEAR Working Group (2005), Decomposition analysis of the BEAR magnetotelluric data: Implications for the upper mantle conductivity in the Fennoscandian Shield, *Geophys. J. Int.*, *163*, 900–914, doi:10.1111/j.1365-246X.2005.02744.x.

Martín Parra, L. M., F. González Lodeiro, D. Martínez Poyatos, and J. Matas (2006), The Puente Génave-Castelo de Vide Shear Zone (southern Central Iberian Zone, Iberian Massif): Geometry, kinematics and regional implications, *Bull. Soc. Geol. Fr.*, *177*, 191–202, doi:10.2113/gssgfbull.177.4.191.

Martínez Catalán, J. R., D. Martínez Poyatos, and F. Bea (2004), Zona Centroibérica: Introducción, in *Geología de España*, edited by J. A. Vera, pp. 68–69, Soc. Geol. Esp.-Inst. Geol. Min. Esp., Madrid.

Martínez Poyatos, D. (2002), Estructura del borde meridional de la Zona Centroibérica y su relación con el contacto entre las Zonas Centroibérica y de Ossa-Morena, Ph.D. thesis, 295 pp., Univ. de Granada, Granada, Spain.

Martínez Poyatos, D., J. F. Simancas, A. Azor, and F. González Lodeiro (1998), Evolution of a Carboniferous piggyback basin in the southern Central Iberian Zone (Variscan Belt, SE Spain), *Bull. Soc. Geol. Fr.*, *169*, 573–578.

Martínez Poyatos, D., F. González Lodeiro, A. Azor, and J. F. Simancas (2001a), La estructura de la Zona Centroibérica en la región de Los Pedroches (Macizo Ibérico meridional), *Rev. Soc. Geol. Esp.*, *14*, 147–160.

Martínez Poyatos, D., F. Nieto, A. Azor, and J. F. Simancas (2001b), Relationships between very low-grade metamorphism and tectonic deformation: Examples from the southern Central Iberian Zone (Iberian Massif, Variscan Belt), *J. Geol. Soc.*, *158*, 953–968, doi:10.1144/0016-764900-206.

Martínez Poyatos, D., M. A. Díez Balda, J. Macaya, F. González Lodeiro, J. R. Martínez Catalán, and R. Vegas (2004), Zona Centroibérica: Dominio del Complejo Esquisto-grauváquico. Estructura: El acortamiento varisco inicial, in *Geología de España*, edited by J. A. Vera, pp. 84–87, Soc. Geol. Esp.-Inst. Geol. Min. Esp., Madrid.

Matte, P. (2001), The Variscan collage and orogeny (480–290 Ma) and the tectonic definition of the Armorica microplate: A review, *Terra Nova*, *13*, 122–128, doi:10.1046/j.1365-3121.2001.00327.x.

McNeice, G., and A. G. Jones (2001), Multisite, multifrequency tensor decomposition of magnetotelluric data, *Geophysics*, *66*, 158–173, doi:10.1190/1.1444891.

Meju, M. A. (1996), Joint inversion of TEM and distorted MT soundings: Some effective practical considerations, *Geophysics*, *61*, 56–65, doi:10.1190/1.1443956.

Monteiro Santos, F. A., J. Pous, E. P. Almeida, P. Queralt, A. Marcuello, H. Mati, and L. A. Mendes Victor (1999), Magnetotelluric survey of the electrical conductivity of the crust across the Ossa Morena Zone and South Portuguese Zone suture, *Tectonophysics*, *313*, 449–462, doi:10.1016/S0040-1951(99)00209-7.

Monteiro Santos, F. A., A. Mateus, E. P. Almeida, J. Pous, and L. A. Mendes Victor (2002), Are some of the deep crustal conductive features found in SW Iberia caused by graphite?, *Earth Planet. Sci. Lett.*, *201*, 353–367, doi:10.1016/S0012-821X(02)00721-5.

Muñoz, G., W. Heise, C. Paz, E. Almeida, F. Monteiro Santos, and J. Pous (2005), New magnetotelluric data trough the boundary between the Ossa Morena and Centroiberian zones, *Geol. Acta*, *3*, 215–223.

Muñoz, G., A. Mateus, J. Pous, W. Heise, F. Monteiro-Santos, and E. Almeida (2008), Unraveling middle-crust conductive layers in Paleozoic Orogens through 3D modeling of magnetotelluric data: The Ossa-Morena Zone case study (SW Iberian Variscides), *J. Geophys. Res.*, *113*, B06106, doi:10.1029/2007JB004987.

Nance, R. D., G. Gutiérrez-Alonso, K. J. Ducan, U. Linnemann, J. B. Murphy, C. Quesada, R. A. Strachan, and N. H. Woodcock (2010), Evolution of the Rheic Ocean, *Gondwana Res.*, *17*, 194–222, doi:10.1016/j.gr.2009.08.001.

Ogawa, Y., A. G. Jones, M. Unsworth, J. Booker, X. Lu, J. Craven, B. Roberts, J. Parmelee, and C. Farquharson (1996), Deep electrical conductivity structures of the Appalachian Orogen in the southeastern U.S, *Geophys. Res. Lett.*, *23*, 1597–1600, doi:10.1029/95GL03601.

Ortega, E. (1986), Geology and metallogeny of the Almadén area, Centro-Iberian Zone, Spain, in *Remote Sensing in Mineral Exploration*, edited by V. Wambeke, *EEC. Rep. 11317*, pp. 147–173, Eur. Econ. Comm., Brussels.

Palomeras, I., R. Carbonell, I. Flecha, J. F. Simancas, P. Ayarza, J. Matas, D. Martínez Poyatos, A. Azor, F. González Lodeiro, and A. Pérez Estaún (2009), Nature the lithosphere across the Variscan orogen of SW Iberia: Dense wide-angle seismic reflection data, *J. Geophys. Res.*, *114*, B02302, doi:10.1029/2007JB005050.

Pous, J., G. Muñoz, W. Heise, J. C. Melgarejo, and C. Quesada (2004), Electromagnetic imaging of Variscan crustal structures in SW Iberia: The role of interconnected graphite, *Earth Planet. Sci. Lett.*, *217*, 435–450, doi:10.1016/S0012-821X(03)00612-5.

Prodehl, C., V. S. Moreira, S. Mueller, and A. S. Mendes (1975), Deep-seismic sounding experiments in central and southern Portugal, paper presented at 14th General Assembly of the European Seismological Commission, Berlin.

Quesada, C., and R. D. Dallmeyer (1994), Tectonothermal evolution of the Badajoz-Cordóba shear zone (SW Iberia): Characteristics and $^{40}Ar/^{39}Ar$ mineral age constraints, *Tectonophysics*, *231*, 195–213, doi:10.1016/0040-1951(94)90130-9.

Raiche, A. P., D. L. B. Jupp, H. Rutter, and K. Vozoff (1985), The joint use of coincident loop transient electromagnetic and Schlumberger sounding to resolve layered structures, *Geophysics*, *50*, 1618–1627, doi:10.1190/1.1441851.

Ribeiro, A., et al. (2007), Geodynamic evolution of SW Europe Variscides, *Tectonics*, *26*, TC6009, doi:10.1029/2006TC002058.

Rodi, W., and R. L. Mackie (2001), Nonlinear conjugate gradients algorithm for 2-D magnetotelluric inversions, *Geophysics*, *66*, 174–187, doi:10.1190/1.1444893.

Simancas, J. F., J. Galindo Zaldívar, and A. Azor (2000), Three dimensional shape and emplacement of the Cardenchosa deformed pluton (Variscan Orogen, southwestern Iberian Massif), *J. Struct. Geol.*, *22*, 489–503, doi:10.1016/S0191-8141(99)00178-9.

Simancas, J. F., et al. (2003), Crustal structure of the transpressional Variscan orogen of SW Iberia: SW Iberia deep seismic reflection profile (IBERSEIS), *Tectonics*, *22*(6), 1062, doi:10.1029/2002TC001479.

Tait, J., M. Schätz, V. Bachtadse, and H. Soffel (2000), Palaeomagnetism and Palaeozoic palaeogeography of Gondwana and European terranes, in *Orogenic Processes: Quantification and Modelling in the Variscan Belt*, edited by W. Franke et al., 4*Geol. Soc. Spec. Publ.*, *179*, 21–34, doi:10.1144/GSL.SP.2000.179.01.04.

Tejero, R., et al. (2008), The ALCUDIA seismic profile: An image of the Central Iberian Zone (southern Iberian Variscides, Spain), *Geo Temas*, *10*, 283–285.

Unsworth, M. J., A. G. Jones, W. Wei, G. Marquis, S. Gokarn, and J. Spratt (2005), Crustal rheology of the Himalaya and southern Tibet inferred from magnetotelluric data, *Nature*, *438*, 78–81, doi:10.1038/nature04154.

Vidal, G., S. Jensen, and T. Palacios (1994), Neoproterozoic (Vendian) ichnofossils from Lower Alcudian strata in central Spain, *Geol. Mag.*, *131*, 169–179, doi:10.1017/S0016756800010700.

Vieira da Silva, N., A. Mateus, F. A. Monteiro Santos, E. P. Almeida, and J. Pous (2007), 3D electromagnetic imaging of a Palaeozoic plate-tectonic boundary segment in SW Iberian Variscides (S Alentejo, Portugal), *Tectonophysics*, *445*, 98–115, doi:10.1016/j.tecto.2007.06.006.

von Raumer, J., G. Stampfli, G. Borel, and F. Bussy (2002), The organization of pre-Variscan basement areas at the north-Gondwanan margin, *Int. J. Earth Sci.*, *91*, 35–52, doi:10.1007/s005310100200.

Wannamaker, P. E., G. R. Jiracek, J. A. Stodt, T. G. Caldwell, V. M. Gonzalez, J. D. McKnight, and A. D. Porter (2002), Fluid generation and pathways beneath an active compressional orogen, the New Zealand Southern Alps, inferred from magnetotelluric data, *J. Geophys. Res.*, *107*(B6), 2117, doi:10.1029/2001JB000186.

Wei, W., et al. (2001), Detection of widespread Fluids in the Tibetan crust by magnetotelluric studies, *Science*, *292*, 716–719, doi:10.1126/science.1010580.

F. Anahnah, D. Martínez Poyatos, A. Pedrera, and A. Ruiz-Constán, Departamento de Geodinámica, Universidad de Granada, s/n, E-18071 Granada, Spain.

J. Galindo-Zaldívar, Instituto Andaluz de Ciencias de la Tierra-CSIC, Universidad de Granada, Campus de Fuentenueva s/n, E-18071 Granada, Spain.

R. Gonçalves, Instituto Politécnico de Tomar, Quinta do Contador, Estrada da Serra, P-2300-313, Tomar, Portugal.

W. Heise and F. M. Santos, Facultade de Ciencias da Universidade de Lisboa, CGUL-IGL, Campo Grande, Ed. C8, P-1749-016 Lisbon, Portugal.

P. Ibarra, Instituto Geológico y Minero de España, La Calera 1, Tres Cantos, E-28760 Madrid, Spain.

A. Mateus, Departamento de Geologia and CeGUL, Faculdade Ciências, Universidade de Lisboa, Campo Grande, C6, Piso 4, P-1749-016 Lisboa, Portugal.

J. Pous, Departament de Geodinàmica i Geofísica, Universitat de Barcelona, s/n, E-08028 Barcelona, Spain. (jpous@ub.edu)